MUTANT p53 RESCUE EFFECACY

Folded protein ↑ : **74 times**

Thermostability ↑ : **6.5 ℃**

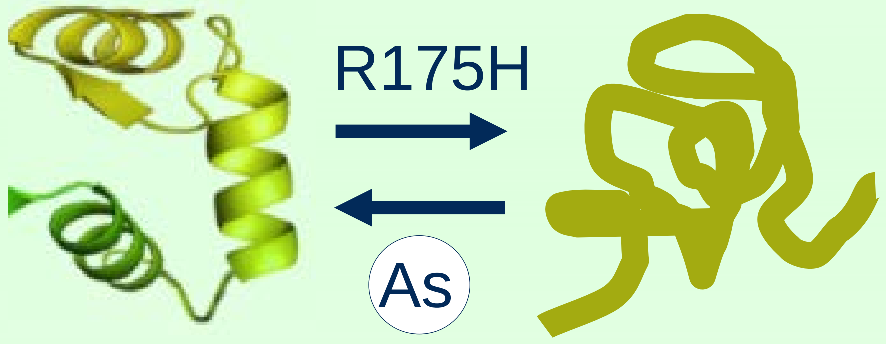

Transactivity ↑ : **44 times**

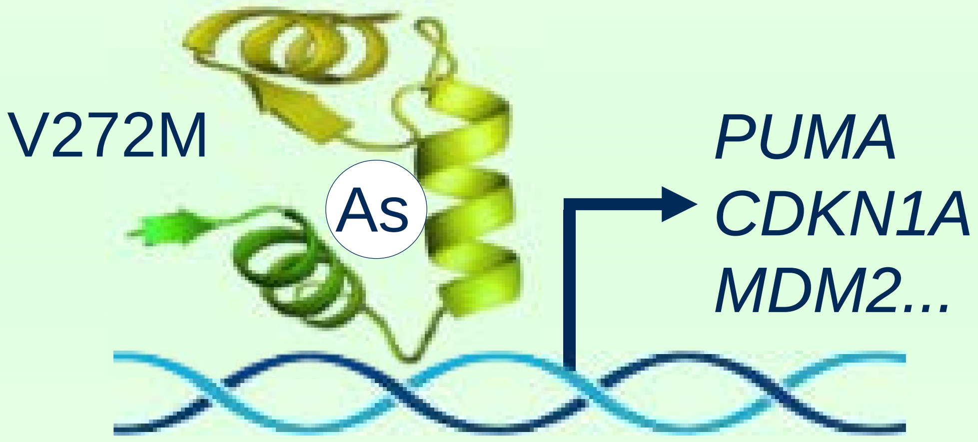

MOLECULAR MECHANISM

Stable ancient p53

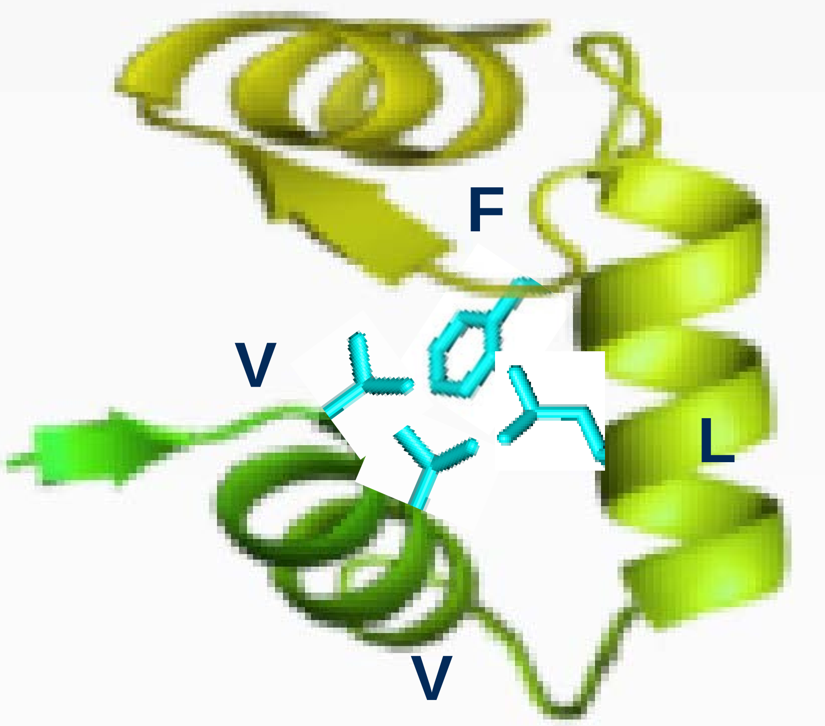

Less stable human p53 and mutants

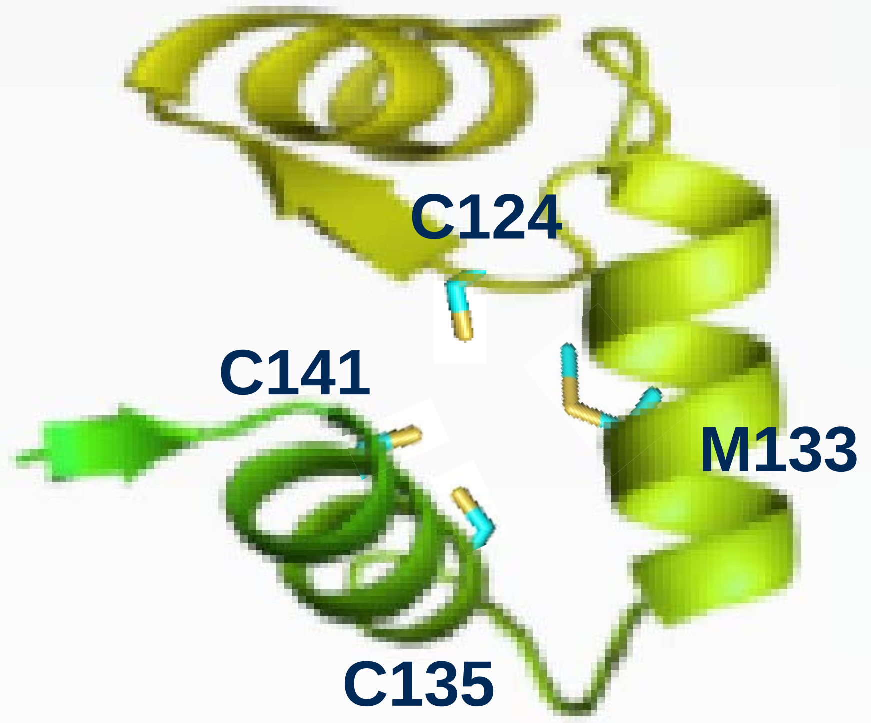

ATO-stabilized p53 mutants

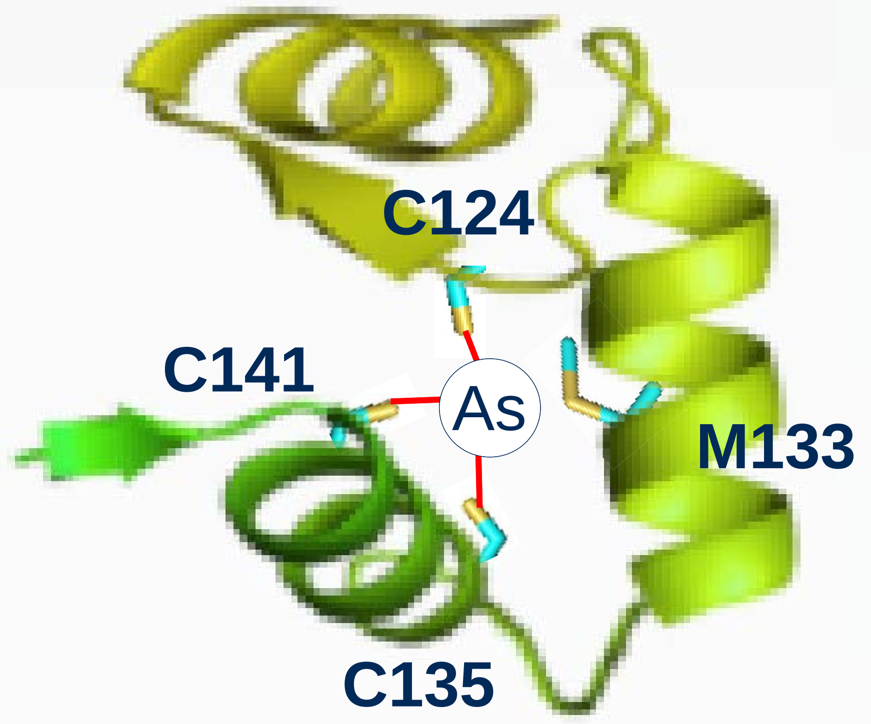

RESCUE PATTERN

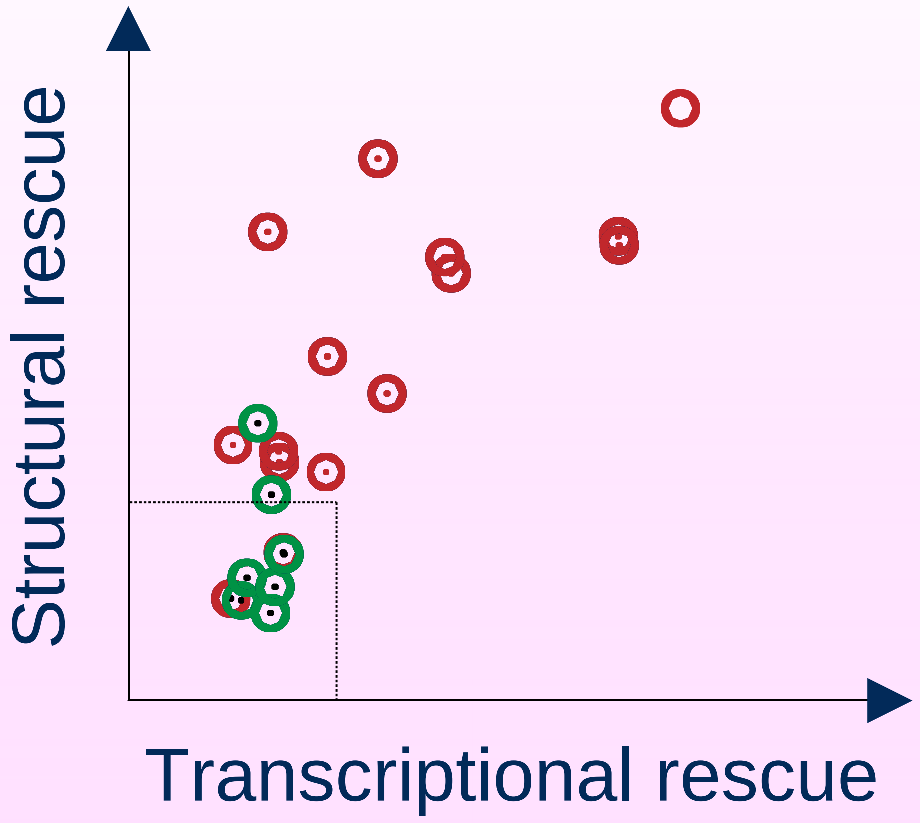

○ DNA-contact p53 mutations
(no rescue)

○ Structural p53 mutations
(universal structural rescue,
diverse transcriptional rescue)

Suggests potential therapeutic value depending on p53 mutation profile in individual patients

Arsenic Trioxide Rescues Structural p53 Mutations through a Cryptic Allosteric Site

Shuo Chen,[1,2,3] Jia-Le Wu,[1,3] Ying Liang,[1,3] Yi-Gang Tang,[1,3] Hua-Xin Song,[1] Li-Li Wu,[1] Yang-Fei Xing,[1] Ni Yan,[1] Yun-Tong Li,[1] Zheng-Yuan Wang,[1] Shu-Jun Xiao,[1] Xin Lu,[2,*] Sai-Juan Chen,[1] and Min Lu[1,4,*]

[1]Shanghai Institute of Hematology, State Key Laboratory of Medical Genomics, National Research Center for Translational Medicine (Shanghai), Ruijin Hospital affiliated to Shanghai Jiao Tong University School of Medicine, Shanghai 200025, China

[2]Ludwig Institute for Cancer Research, Nuffield Department of Medicine, University of Oxford, Oxford OX3 7DQ, UK

[3]These authors contributed equally

[4]Lead Contact

[*]Correspondence: min.lu@shsmu.edu.cn (M.L.), xin.lu@ludwig.ox.ac.uk (X.L.)

SUMMARY

TP53 is the most frequently mutated gene in cancer, yet these mutations remain therapeutically non-actionable. Major challenges in drugging p53 mutations include heterogeneous mechanisms of inactivation and the absence of broadly-applicable allosteric sites. Here we report the identification of small molecules including arsenic trioxide (ATO), an established agent in treating acute promyelocytic leukemia, as cysteine-reactive compounds that rescue structural p53 mutations. Crystal structures of arsenic-bound p53 mutants reveal a cryptic allosteric site involving three arsenic-coordinating cysteines within the DNA-binding domain, distal to the zinc-binding site. Arsenic binding stabilizes the DNA-binding loop-sheet-helix motif alongside the overall β-sandwich fold, endowing p53 mutants with thermostability and transcriptional activity. In cellular and mouse xenograft models, ATO reactivates mutant p53 for tumor suppression. Investigation of the most frequent twenty-five p53 mutations informs patient stratification for clinical exploration. Our results provide mechanistic basis for repurposing ATO to target p53 mutations for widely-applicable yet personalized cancer therapies.

INTRODUCTION

Large-scale cancer genome studies have converged on *TP53*, which encodes the tumor suppressor and transcription factor p53, being the most commonly mutated gene in human cancer (Kandoth et al., 2013; Zehir et al., 2017), yet p53 mutations remain hitherto therapeutically non-actionable (Levine, 2019).

Distinct from mutations in oncogenes such as *KRAS* and *PIK3CA* that cluster at a codon or two, the majority of *TP53* mutations are missense in cancer with a wide codon distribution (Olivier et al., 2010; Zehir et al., 2017). Crystallographic analysis of p53–DNA interactions suggested divergent structural mechanisms of inactivation by missense mutations (Cho et al., 1994; Joerger and Fersht, 2008). Some of these p53 mutations (such as those at mutational hotspots Arg248 and Arg273) eliminate direct DNA contacts, whereas many of the remaining mutations compromise the wild-type DNA-binding domain (DBD) structure, first termed structural p53 mutations (such as those at hotspots Arg175, Gly245, Arg249, and Arg282) (Cho et al., 1994). It is therefore a formidable challenge to rescue p53 mutations of heterogeneous inactivating mechanisms with a single agent.

A further complication of drugging p53 mutations is the absence of an established allosteric regulatory site of broad applicability within its DBD. Targeting the zinc-coordination site for drug development has proven problematic, although a lead compound that delivers zinc showed p53-R175H-specific activities (Yu et al., 2012). One noteworthy site, albeit unique to Y220C, involves a surface crevice away from the DNA-binding surface (Joerger et al., 2006). A class of related small molecules have been developed that insert into the crevice, thereby stabilizing this p53 mutant (Boeckler et al., 2008; Joerger and Fersht, 2010). Regrettably this Y220C-specific binding cleft is not applicable to other p53 mutants.

Over the past decades, myriad lead compounds that show potential in rescuing cancer-derived p53 mutations have been identified (Joerger and Fersht, 2016; Levine, 2019). Many of these compounds, including the clinical-stage APR-246 (PRIMA-1^{MET}, a derivative of PRIMA-1) (Bykov et al., 2002; Bykov et al., 2005) share the intriguing feature of the capacity to bind thiol groups of cysteines (Joerger and Fersht, 2016; Olivier et al., 2010). With this inspiration, we further hypothesized that compounds capable of binding multiple cysteines could stabilize p53 when the DBD fold is compromised by structural mutations (Figure 1A). We set out to identify generic compounds that could rescue structural p53 mutations, which collectively account for more than half of all p53 alterations.

RESULTS

Identification of Arsenic Compounds

We devised a screen to seek small molecules that rescue structural p53 mutations through binding multiple cysteines (Figure 1B). We first mined data from the NCI-60 Human Tumor Cell Lines Screen for compounds that preferentially inhibit the growth of cell lines with p53 mutations at structural hotspots (five lines: RXF 393 [R175H], CCRF-CEM [R175H/R248Q], HOP-92 [R175L], SK-MEL-2 [G245S], and BT-549 [R249S]) (referred to as sensitive cell lines; Figures 1B and S1A; Table S1). In the NCI-60 ensemble there are 14 cell lines that are wild-type for p53 and a further 15 lines with other types of p53 defects (including mutations of residues that contact DNA), which we deemed insensitive to the desired compounds (Figure S1A; Table S1). The remaining 26 cell lines were excluded from the analysis because of either inconclusive p53 status or less-characterized p53 missense mutations (Figure S1A; Table S1). Contrary to the 29 insensitive cell lines, we found 1,868 small molecules that preferentially inhibited the growth of the five cell lines with structural p53 hotspot mutations (correlation score > 0.3, P value $\leq$ 0.05) (Figure 1B; see Figures 1C and 1D for examples, and Figure 1E for a control; Table S2) using CellMiner (Reinhold et al., 2012), out of the 20,861 Developmental Therapeutics Program (DTP) (Shoemaker, 2006) compounds after quality control.

Based on the proposed thiol-binding substructures (Figure S1B; substructures 5 and 8 potentially bind multiple cysteines whereas the others could only bind one cysteine), we predicted 486 compounds with potential to simultaneously bind multiple cysteines from the 1,868 compounds noted above (Figure 1B and S1B; Table S2; selection criterion: containing substructure 5 or 8, or at least two of substructures 1–8; see

Figure 1C for examples). Out of the 486 compounds identified in the *in silico* screen, we were only able to acquire 64 commercially (Table S2). They were used to treat H1299 cells (null for endogenous p53) transfected with p53-R175H, a prototypic structural p53 mutant allele as well as the most common p53 mutation (Figure 1A). Treated cells were assayed for reactivity to the well-characterized PAb1620 antibody (Figures 1F and S1C; see Figure S1D for data for all 64 compounds), which preferentially recognizes folded p53 (such as the wild-type p53 and p53-R273H) (Wang et al., 2001).

Our pipeline identified four candidate compounds (Figure 1C). NSC90616 contains two α,β-unsaturated carbonyls, a thiol-binding substructure found in many reported mutant p53 rescue compounds (Figure S1E) (Joerger and Fersht, 2016). Intriguingly, all the other three compounds—NSC3060 ($KAsO_2$), NSC92859 (arsenic trioxide/ATO), and NSC405640—contain thiol-binding metals (Figure 1C). As a control, Nutlin-3a—an inhibitor of the MDM2–p53 interaction—selectively inhibits the growth of cell lines with wild-type p53 (Figures 1D and 1E; Table S3) (Vassilev et al., 2004). Our procedure did not identify PRIMA-1 or NSC319726 in the DTP repositories (Figure S1F; Table S3), presumably due to their activities on different spectrums of p53 mutations (for example, including those at DNA-contacting Arg273 for PRIMA-1 and R175H-exclucivity for NSC319726) (Bykov et al., 2002; Yu et al., 2012). In the PAb1620 immunoprecipitation (IP) assay, ATO and $KAsO_2$ induced striking promotion of p53-R175H folding while NSC405640 and NSC90616 displayed much weaker activities (Figures 1F and S1D).

ATO is a clinical antineoplastic drug for treating acute promyelocytic leukemia (APL), through targeting the oncogenic PML-RARα (Zhang et al., 2010). We thus proceeded with evaluating the effects of ATO on folding of the four structural p53 hotspot mutants found in the aforementioned five NCI-60 cell lines. Consistent with previous findings

(Bullock et al., 2000), p53-G245S and p53-R249S displayed more PAb1620 epitope than p53-R175H before ATO treatment (Figures 1G). ATO demonstrated effectiveness in increasing PAb1620 reactivity for all four tested structural p53 mutants, to levels comparable to wild-type p53 (Figure 1G). To systematically evaluate ATO-mediated conformational rescue of endogenous mutant p53, we collected a panel of cancer cell lines expressing mutant p53 covering all six mutational hotspots (Figure 1A) for IP with PAb1620 alongside PAb240, a classical p53 antibody that specifically recognizes unfolded DBD (Cho et al., 1994; Gannon et al., 1990) (Figures 1H and S1G). Upon ATO treatment, loss of PAb240 reactivity was always juxtaposed with gain of PAb1620 reactivity for each and every structural hotspot p53 mutant, regardless of cell lines used (Figures 1H and 1I). Moreover, ATO was able to promote the folding of p53-R172H (the murine equivalent of human p53-R175H) in mouse embryonic fibroblasts (MEFs) as assayed using appropriate antibodies (Figures 1H and 1I). A dose titration showed that as low as 0.1 µg/mL ATO was sufficient to promote p53-R175H folding (Figure S1H), which compares well with the ATO concentrations used in assays for APL-derived NB4 cells (Chen et al., 1997; Chen et al., 1996), and the promotion occurred as soon as 15 min after ATO administration (Figure S1H). Therefore, our multi-tier screen identified arsenic-containing compounds effectively reactivating the most frequent structural p53 mutants.

ATO Stabilizes p53 Folding by Covalent Binding

We next compared ATO to reported mutant p53-reactivating compounds (after concentration optimization for each compound, see Figure S2A) in folding p53-R175H in the PAb1620 IP assay (Figure 2A). In line with earlier reports (Bykov et al., 2002; Yu et al., 2012), we observed increases of PAb1620 epitope to 1.9 fold for PRIMA-1 and 2.6 fold for NSC319726 (Figure 2A). Remarkably, ATO increased PAb1620 reactivity of p53-R175H to ~74 fold, close to wild-type p53 (Figure 2A). PhiKan083 was reported as an allele-specific reactivating compound for Y220C (Boeckler et al., 2008). PhiKan083 did not promote PAb1620 reactivity of p53-R175H in our assay, yet stabilized p53-Y220C to ~2.7 fold (Figure S2B).

Classically, structural p53 mutations are considered to compromise the wild-type DBD structure and reduce thermodynamic stability (Bullock and Fersht, 2001). To assay directly the ATO-induced thermal stabilization of p53, we purified recombinant p53 DBD constructs with the four most frequent cancer-derived structural mutations (Figure 1A), and measured their thermodynamic stabilities using differential scanning fluorimetry (DSF) (Figure 2B). The assay conditions were probed with R175H (Figures S2C–S2E). In accordance with published results (Bullock et al., 2000) and our PAb1620 data (Figures 1G–1I), R175H is highly destabilizing whereas G245S is moderately destabilizing in the DSF assay (Figures 2B for assays using buffer with 150 mM NaCl added; Figure S2F for those without supplemented NaCl). ATO raised the melting temperature (T_m) of the tested mutant p53 DBDs by 0.9–6.5 °C (Figure 2B and S2F). Intriguingly, we found that less ATO was needed to plateau DBD stabilization for R282W than R175H (Figures 2B, S2F, and S2G). In this assay we also benchmarked ATO against the panel of mutant p53-reactivating compounds, and ATO demonstrated substantial stabilizing effects compared to the other compounds for the four mutant DBDs (Figure 2C).

Structural mutation-induced p53 destabilization and aggregation contribute to its loss of tumor-suppressive functions in cancer (Wilcken et al., 2012). In an aggregation assay based on thioflavin T binding, ATO rescued mutation-expedited aggregation of p53 DBD, except G245S (Figures 2D and S2H). In addition, we assessed endogenous p53-R175H in Detroit 562 cells in a glutaraldehyde (GA) fixation-based aggregation assay (Friedman et al., 1993), where ATO apparently decreased full-length R175H aggregation in a dose-dependent manner (Figure 2E).

We next investigated p53 DBD–ATO interactions by mass spectroscopy (MS). In denaturing MS, ATO incubation led to an increase in molecular weight of ~72 dalton (Da) for the four structural p53 DBD mutants (Figures 2F and S2I). A likely scenario is covalent binding between p53 and As atom (75 Da) accompanied with loss of 3 protons. Indeed, other As-containing compounds, such as AsI_3, were also able to induce clear As incorporation into p53 DBD mutants (Figure S2J). We noted differences among the mutants in bound As, which mirrored what we observed in the DSF assay (Figures 2B, 2F, S2F, and S2I). We next explored the DBD–ATO interaction in native MS. p53-R249S retained a zinc (Zn) atom (Figure 2G, upper panel), which was lost under the denaturing condition (Figure 2F, upper panel). Notably, p53-R249S incubated with ATO appeared to have a Zn atom and an As atom bound simultaneously in native MS (Figure 2G, lower panel), suggesting concurrent As and Zn binding to p53 at two distinct sites.

Crystal Structures of As-Bound p53 Mutants

In pursuit of the mechanism of As-mediated structural stabilization, we determined the crystal structures of two representative As-bound p53 DBD mutants (G245S and R249S; Table S4). Unfortunately, we did not manage to crystallize R175H DBD, despite substantial stabilization by ATO. ATO-soaked DBD-G245S crystals permitted structure determination at 2.15 Å (Figure S3A, four copies in the crystallographic asymmetric unit), and AsI_3-incubated DBD-R249S crystals at 1.75-Å resolution (Figure S3B, two copies in the asymmetric unit). Each of the DBD molecules in our final models has a Zn atom bound at the expected Zn-coordination site and an As atom bound in a cryptic binding site (Figures 3A–3C and S3). Overall, the As complexes superpose well with published p53 DBD structures (Figures S3C–S3H).

In the As-bound G245S DBD, Ser245 adopts a modestly unfavorable main chain conformation and orientates its hydroxyl group, which displaces a structural water molecule, towards the zinc-binding site of p53 (Figure 3D). In addition, G245S induces a flip of the peptide bond between Met243 and Gly244, as observed previously (Figure 3D) (Joerger et al., 2006). In As-bound R249S DBD, the L3 loop of one DBD molecule assumes an extended conformation, whereas the one from the other DBD molecule is disordered in the crystal structure (Figure 3E). In both copies, the hydroxyl group of Ser249 replaces a structural water molecule in the hydrogen bond network between the L2 and L3 loops, as described previously (Suad et al., 2009). Intriguingly, there is an intermolecular salt bridge between Arg174 from the p53 molecule with a disordered L3 and Glu171 from the other p53 molecule (Figure 3F). In the wild-type p53 DBD, this Glu171 forms an intramolecular salt bridge with Arg249 (Figure 3F). In summary, the As-bound G245S and R249S DBDs superpose well with wild-type DBD at global folding, however retain alternation at local DNA-binding L3 loop.

The As-Binding Pocket

In each of the six DBDs, for both G245S and R249S, an As atom is evidently coordinated by Cys124, Cys135, and Cys141 (Figures 4A, 4B, and S3). In addition, the side chain of Met133 orientates towards As and makes van der Waals interactions with the As atom (Figures 4A and 4B). These four sulphur-containing p53 residues define the As-binding pocket (ABP). The ABP situates at the joint between the β-sandwich scaffold and the DNA-binding LSH motif (Figure 4C), in the vicinity of the DNA-binding surface (Figure 3A), and thus is well-positioned to function as an allosteric regulatory site. The side chains of the ABP residues are packed between the S2–S2’ hairpin of the LSH motif and the S3 and S8 strands of the opposite β sheet of the core sandwich fold, contributing to the hydrophobic interactions that stabilize the LSH motif and the β sandwich, and their juxtaposition (Figures 4C and 4D). While three out of the four Zn-coordinating residues are solvent-accessible, the ABP is cryptic with only Cys124 being surfaced-exposed (Figure 4E).

The covalent interactions of As with the coordinating cysteines result in a pronounced reorganization of the binding pocket (Figure 4F). Specifically, Cys141 adopts one of two favored alternative conformations to bind As. This Cys141 rotamer points towards Met133, which in turn displays a preferred rotamer conformation that avoids steric clash (Figure 4F, left panel). Cys135 rotates away from the usual As-free conformation and appears to adopt two rotamer conformations to bind As (Figure 4F, right panel). In both cases, the sulphur atoms of the cysteines form the bases of triangular pyramids with As at the apex of each pyramid (Figures 4A, 4B, and 4F).

Mechanism of Regulation and Rescue

We proceeded to investigate the As-binding allosteric site in ATO-mediated rescue. As expected, single alanine substitution of each of the three As-coordinating cysteines (Figure 4G) and concurrent alanine substitutions of Cys135 and Cys141 (C135A/C141A) (Figure 4H) largely prevented ATO-mediated display of the PAb1620 epitope on p53-R175H. Conversely, mutations of the other two cysteine clusters (C238A/C242A and C275A/C277A) in the p53 DBD did not appreciably diminish As-induced PAb1620 reactivity (Figure 4H).

Previous efforts to engineer stabilizing p53 mutations inspired by evolution converged on alterations of ABP residues, including M133L (Nikolova et al., 1998), C135V (Petty et al., 2011), and C141V (Petty et al., 2011) (Figure S4). In line with these findings, in our PAb1620 assay, valine substitutions C135V, C141V, and, to a lesser extent, C124V all increased the PAb1620 reactivity of p53 mutant R175H (Figure 4I). A leucine at position 133 coupled with a tryptophan at codon 124 seems a prominent feature of p63, p73, and some invertebrate p53 orthologues (Figures 4J), and an apparently favorable arrangement for structural stability (Figures 4K).

Therefore, the covalent As incorporation at the ABP seems to compensate for the relatively small and less hydrophobic side chains of cysteines in this hydrophobic pocket of human p53, in a way similar to the bulkier and more hydrophobic residues found at equivalent positions throughout evolution. It locks the side chains of the ABP residues in position, thereby stabilizing the LSH motif, the β-sandwich fold, and notably the anchor of LSH to the β sandwich integrating the LSH motif with the β-sandwich backbone into a rigidified DNA-binding posture.

Transcriptional Reactivation by ATO

Transcriptional activities are central to p53-mediated tumor suppression. In a classical luciferase reporter assay, ATO preferentially reactivated the structural mutants on the representative p53 response elements (REs) of *BBC3*/*PUMA* and *CDKN1A* in p53-null H1299 cells (Figures 5A and S5A). In comparison, the effects of ATO on the DNA-contact mutants were less pronounced. More detailed analyses of the structural mutant R282W showed ATO-mediated transcriptional reactivation in all tested cell lines despite RE- and cell line-specific variations (Figure 5B), and in a dose-dependent manner (Figure 5C). Consistent with structural observations, alanine substitution of each of the As-coordinating cysteines largely abolished the reactivation of R282W by ATO (Figure 5D). As discussed above, the surface-exposed As-coordinating Cys124 of human p53 is substituted with a tryptophan in paralogs p63 and p73, and ATO did not rescue p53 R282W-equivalent mutation in p63 (R352W) (Figure 5E, left panel).

p63(CMCC)-R352W (p63-R352W with the p53 ABP-equivalent residues) was transcriptionally rescued by ATO, and p53(WLCC)-R282W (p53-R282W with p63-equivalent residues at the ABP) was not (Figure 5E, right panel).

To demonstrate reactivation of endogenous mutant p53 by ATO, we further assayed expression of classical p53 transcriptional targets at RNA (Figures 5F and S5B) and protein (Figures 5G and S5C) levels using the panel of cancer cell lines tested in the IP experiment (Figure 1H). Broadly speaking, reactivation of the tested p53 targets (p21, PUMA, and MDM2) was evident in cell lines with structural p53 mutants but was less marked in those with DNA-contact mutants (Figures 5F, 5G, S5B, and S5C; summarized as Figure S5D), consistent with the reporter assay.

ATO Reactivates Mutant p53 for Tumor Suppression

We next used cell line-derived xenograft (CDX) and patient-derived xenograft (PDX) mouse models to study mutant p53 reactivation by ATO in tumor suppression. 5 mg/kg ATO was used because this dosage was widely used in APL mouse models (Jing et al., 2001; Lallemand-Breitenbach et al., 1999). In addition, this dosage yielded 0.05–0.2 µg/ml As plasma concentration in mice (Hughes et al., 1999; Modi et al., 2005), which can be achieved in ATO-treated APL patients without profound toxicity (Hu et al., 2009; Zhu et al., 2013).

CEM-C1 cells expressing endogenous p53-R175H—which showed ATO-mediated rescue in our cellular assays (Figure S5D)—was tested in the CDX model. CEM-C1 cells were intravenously injected into the NOD/SCID mice on day 1 (Figure 6A and S6A). CEM-C1 (human CD45+) clonal expansion was detectable in peripheral blood (PB) at day 22, accounting for > 0.05% of PB cells (Figures 6B and S6B). Daily administration of ATO from day 23 onwards significantly extended the lifespan of ATO-injected mice with a median survival increased from 32 to 46 days (Figure 6C). The lifespan extension of ATO-treated mice inversely associates with CEM-C1 clonal expansion in PB as the averaged percentages of CEM-C1 cells in PB on day 26 are 0.6% in the control mice and 0.1% in the ATO-treated mice (Figure 6B and S6B).

To investigate further whether ATO is able to suppress solid tumor growth by reactivating p53-R175H, we used an engineered H1299 cell line (p53-R175H-Tet-Off), in which the expression of p53-R175H can be silenced by doxycycline (Dox) treatment (Figure S6C) (Yap et al., 2004). We confirmed that ATO could restore transcriptional activity to p53-R175H (Figure S6D), induced the protein expression of p53 targets (Figures S6E), and reduce cell viability (Figure S6F). With this *in vitro* confirmation, the H1299 p53-R175H-Tet-Off cells were subcutaneously injected into nude mice on day 1 and tumor growth was monitored (Figures 6D and S6G). From day 21 onwards, ATO was administered daily. The most profound tumor-suppressive impact of ATO was observed in high p53-R175H expressing H1299 tumors (without Dox treatment; Figures 6E and 6F). Despite large variations, the averaged tumor size and tumor weight of ATO-treated high p53-R175H-expressing H1299 tumors on day 48 were approximately 10–20% of those of untreated tumors (Figures 6E, 6F, and S6H). Addition of Dox in drinking water resulted in low p53-R175H-expressing H1299 tumors (Figure 6E), wherein ATO had minimal impact on the averaged tumor size and tumor weight (Figures 6E, 6F, and S6H). These results illustrated that ATO suppresses tumor growth by reactivating p53-R175H.

We next employed non-small cell lung carcinoma (NSCLC) PDX harboring p53-R282W. Initially, 48 nude mice were inoculated with NSCLC tumor tissues on day 1 (Figures 6G and S6I). On day 37, 16 mice with similar tumor sizes were selected to carry out randomized drug treatment to minimize the variation in initial tumor sizes caused by heterogeneity among mice. Treatment with ATO daily reduced tumor size and weight by 42.9% and 25.6%, respectively, on day 57, with minimal effect on mouse body weight (Figures 6G, 6H, S6J, and S6K). Cisplatin, a first-line chemotherapeutic agent for NSCLS in clinics, was used as a positive control. Interestingly ATO and cisplatin suppressed tumor growth at a similar level (Figures 6G, 6H, and S6K), and neither treatment affected the amount of p53-R282W detected in the isolated tumors, using immunoblotting and immunohistochemistry staining (Figures 6I–6K). Upregulation of p21 was mainly detected in ATO-treated but not in cisplatin-treated PDX tumors (Figures 6I–6K). In contrast, enhanced γ-H2A.X (phosphorylated Ser139 H2X, a marker of DNA damage) expression was more profound in cisplatin- but not in ATO-treated tumors in comparison to PBS controls. Thus, ATO and cisplatin likely suppressed tumor via different mechanisms. Taken together, ATO has the potential to treat leukemia more widely as well as inhibit solid tumor growth *in vivo*, which we attribute, at least in part, to ATO reactivating structural mutant p53.

Applicable Spectrum of p53 Mutations

We next assessed the 25 most frequent p53 mutations found in cancer (Figure 7A; as collated in the IARC, R19) for ATO-mediated rescue. These 25 mutant alleles collectively account for 40.87% of p53 missense mutations in cancers, and all map to the p53 DBD (Figures 7A and S7A). Our structural analysis of these mutations predicted that all, except mutations at DNA-contacting Ser241, Arg248, and Arg273, compromise the wild-type p53 structure. Indeed, all the 19 structural p53 mutants showed reduced PAb1620 reactivities, most of which are rescued, albeit to varying extents, by ATO (Figures 7B). Apparently, mutations V157F, R158H, Y205C, and Y220C, which are distant from the As-binding site and in the vicinity of the PAb1620 epitope (Wang et al., 2001), were not rescued by ATO in PAb1620 IP (Figures 7B), yet it is not clear whether these results reflected overall p53 folding or local structural changes that precluded PAb1620 binding. Intriguingly, specific mutant alleles affecting DNA-contacting p53 residues (S241F and R248W) displayed attenuated PAb1620 IP signals (Figure 7B), in line with a previous proposal that certain DNA-contact p53 mutants are also structural (Bullock and Fersht, 2001; Wong et al., 1999). The folding of these mutants appeared to be partially rescued by ATO (Figure 7B).

In the luciferase reporter assay, ATO did not significantly reactivate any DNA-contact p53 mutants (Figure 7C). In contrast, the structural p53 mutations V272M, R282W, E285K, and Y234C were rescued potently by ATO in transactivation (Figure 7C). Curiously, these mutations showed less impressive absolute increases in PAb1620 reactivity (Figure 7B). We speculate that such LSH mutations have disproportional impacts on PAb1620 recognition because of the DBD topology (i.e. strand 10 connecting a loop in the vicinity of PAb1620 epitope to the C-terminal helix). This notion is further supported by PAb240 analysis where such mutants demonstrated substantial loss of PAb240 reactivity upon ATO treatment, similar to R175H (Figures 1H, 1I, and S7B). Of note, these mutations were described as more promising targets for rescue by generic small-molecule drugs (Joerger et al., 2006). The remained mutations, such as R249S and G245S, were rescued with transcriptional activity to considerably varying degrees.

We then investigated reactivation of mutant p53 by ATO in growth inhibition of cancer cell lines (Figure 7D). ATO showed significantly stronger killing towards the cancer cell lines with structural p53 mutations (Figure 7D). We noticed some lines without structural p53 mutations were also somewhat sensitive to ATO treatment by showing IC_{50} < 1 μg/ml (Figure 7D, right panel), such as the MDA-MB-468 harboring the R273H mutant that was not rescued by ATO in our other assays. This implies p53-independent effects of ATO in inhibiting cancer cells. To ascertain the involvement of mutant p53 in ATO-mediated growth inhibition, we ablated p53 using siRNA in these cells (Figure 7E). The ablation of p53 substantially increased IC_{50} of ATO in Loucy, but not in MDA-MB-468 or A431. Therefore, growth inhibition by ATO is in part mediated by p53-V272M in Loucy, but not apparently associated with p53-R273H in either MDA-MB-468 or A431. We next characterized endogenous V272M and R273H activities in response to ATO (Figures 7F–7H). In the ChIP-qPCR assay, we found elevated binding of V272M to all tested p53 response elements (REs) in Loucy, but not for the R273H mutant in MDA-MB-468 or A431 (Figure 7F and S7C). In line with the ChIP results, we found significant upregulation of the p53 targets on RNA and protein levels in Loucy, but not in MDA-MB-468 or A431 (Figures 7G and 7H). Similar observations were also made in other cancer cell lines (LK2 and TE-1) expressing endogenous V272M (Figures S7D–S7F).

To enable a glimpse of the transcription reactivation profiles by ATO, we generated two isogenic cell lines in which p53-deleted HCT116 cells were introduced with either p53-R282W or p53-V272M, two mutants transcriptionally reactivated by ATO. These two isogenic lines were treated with ATO, followed by RNA sequencing (Figure 7I). Among the 116 consensus p53 targets (Fischer, 2017), the majority are upregulated by ATO in both V272M and R282W lines (Figures 7I and S7G; Table S5). The two transcription profiles are highly correlated ($r = 0.61$ and $P = 0.00$) yet exhibit mutant-specific signatures (Figures 7I, S7G, and S7H). Intriguingly *RCHY1*, encoding p53-regulated ubiquitin ligase Pirh2 that promotes p53 degradation, was upregulated by ATO (Figure S7G), in line with previous reports (Yan et al., 2014; Yan et al., 2011). In the pathway enrichment analysis for ATO-upregulated genes in NCI-Nature and Panther databases, direct p53 effectors and p53 pathway were the most enriched pathways, respectively (Figure S7I).

DISCUSSION

Here we report that As binds to a cryptic cysteine triad to rescue structural p53 mutants. It is noteworthy that As-binding cysteine triad may exist in other proteins and contribute to p53-independent anti-cancer activity or toxicity of ATO (Kitchin and Wallace, 2006). A typical example is the one in the oncogenic PML-RARα fusion protein in APL (Zhang et al., 2010). Notably, the specific binding of As to the cysteine triad of ABP pocket is distinct from other single cysteine-reactive p53 rescue compounds such as APR-246 (Zhang et al., 2018), which promiscuously bind spatially-distant, surface-exposed cysteines.

Based on the extrapolation on the 25 most frequent p53 mutations, ATO has the potential to rescue a broad spectrum of p53 mutations in cancer (Figures 7J and 7K; 22.7%, 1.3%, and 34.3% of missense mutants were rescued in structural stability, transcriptional activity, and both, respectively). Despite the universal structural rescue among structural mutants, their transcriptional activity was not always efficiently rescued. Crystal structures of three hotspot mutants upon global refolding provide some clues—the efficiently rescued R282W mutant retains intact DNA-binding surface (Joerger et al., 2006) whereas in our study R249S and G245S mutants that are less efficiently rescued retain local alternations at the DNA-binding surface. Thus, the integrity of local DNA-binding surface, in addition to global folding, apparently determines the efficiency of ATO-mediated transcriptional activity rescue. In relation to precisely recruiting cancer patients that most likely benefit from ATO treatment, quantitative determination of ATO rescue efficiencies for the hundreds of structural p53 mutations is optimal.

Curing APL with ATO in combination with retinoid acid has provided a paradigm for targeted cancer therapies (de The et al., 2017; Wang and Chen, 2008). Encouragingly, therapeutic potential of ATO was reported in other hematological (Hu et al., 2020; Wang et al., 2013) and some solid tumors (Wang et al., 2015; Wang et al., 2017) in clinics. Anti-cancer activity of ATO was also reported in p53-mutated cancer cells *in vitro* (Liu et al., 2003; Yan et al., 2014; Yan et al., 2011). Our study, alongside these previous works, suggests potential of repurposing ATO in treating p53-mutated cancer patients. A phase I PANDA (P53 AND As) clinical trial for p53-mutated hematological malignancy patients is ongoing (NCT03855371).

ACKNOWLEDGEMENTS

We thank staff of the BL17U/BL18U1/BL19U1/BL19U2/BL01B beamlines of National Center for Protein Science Shanghai (NCPSS) at Shanghai Synchrotron Radiation Facility (SSRF) and Dong-Ming Qian of Viva Biotech for technical assistance. We thank the high throughput screening core, National Research Center for Translational Medicine (Shanghai) for library screening. We are grateful to Mary Muers, Yvonne Jones, and Zhu Chen for critical reading of the manuscript. M.L. was funded by the National Key R&D Program of China (2017YFA0506200), the National Natural Science Foundation of China (81622002 & 81861130368 & 82073292), the Clinical Research Program of Ruijin Hospital (2018CR006), the Shanghai Education Commission–Gaofeng Clinical Medicine Grant (828318 & 20161305), the Shanghai Youth Talent Development Program (2017275), the Shanghai Excellent Youth Academic leader (20XD1422700), the Shanghai Medical and Health Excellent Discipline Leader Development Plan (2018BR36), the Shanghai Collaborative Innovation Center for Translational Medicine (TM201902), the Foundation of National Facility for Translational Medicine (Shanghai) (TMSK-2020-003), and the Newton Advanced Fellowship (NAF\R1\180216). S.C. and X.L. were funded by the Ludwig Institute for Cancer Research.

AUTHOR CONTRIBUTIONS

M.L. conceived the study and designed all experiments. M.L. and S.-J.C. supervised the project. S.C., J.-L.W., Y.L., Y.-G.T., H.-X.S., Y.-F.X., N.Y., Y.-T.L., Z.-Y.W., S.-J.X., L.-L.W., and M.L. performed the experiments. S.C., X.L., and M.L. analyzed the data. S.C., X.L., S.-J.C., and M.L. wrote the manuscript.

DECLARATION OF INTERESTS

M.L., J.-L.W., and H.-X.S. are co-authors of the pending patents ‘PANDA as a novel therapeutic’ (PCT/CN2018/085190), and ‘mp53 rescue compounds and methods of treating a p53 disorder’ (PCT/CN2019/070117). The authors declare no other competing interests.

FIGURE LEGENDS

Figure 1. Identification of arsenic compounds

(A) Codon distribution of nonsynonymous *TP53* mutations (IARC; R18) (top left), the most frequent mutations (bottom left), and locations of p53 mutational hotspots and cysteines mapped onto a p53–DNA complex (PDB: 1TUP).

(B) Screen overview.

(C) Chemical structures of the 4 compounds identified from the screen.

(D and E) Plot graphs of the GI_{50} of the indicated compounds on the NCI-60 cell lines. See STAR Methods for details.

(F and G) PAb1620 IP for the 4 hits. H1299 cells expressing the indicated p53 mutants were treated with compounds overnight (1 μg/ml ATO used unless otherwise indicated); cells were lysed, followed by PAb1620 IP and immunoblotting using DO1 and a secondary antibody that specifically recognizes the light chain.

(H and I) PAb1620, PAb240, and PAb246 IP for cells expressing endogenous p53. (H) Cells were treated with ATO overnight, followed by IP using the indicated antibodies. Representative immunoblotting from two biological replicates was shown. (I) The signal density ratios of the immunoprecipitated p53 in (H) were quantified. Bars represent mean (n = 2).

See also Figure S1 and Table S1 – S3.

Figure 2. ATO stabilizes p53 by covalent binding

(A) PAb1620 IP assay for p53-R175H in H1299 cells. Cells were treated with the indicated compounds overnight under the concentrations shown in brackets (μg/mL). Bar graph shows the mean PAb1620 IP efficiency (n = 2).

(B) Recombinant p53 DBDs were mixed with ATO at indicated ratios in 20 mM HEPES (pH 7.5) containing150 mM NaCl overnight. Melting curves were measured by DSF. Right panel shows the calculated T_m.

(C) Calculated T_m of p53-R175H upon incubation with the indicated compounds in 20 mM HEPES (pH 7.5) overnight.

(D) The indicated DBDs after ATO incubation was mixed with thioflavin T dye. Aggregated protein signal was measured at 37°C for 1 h.

(E) Detroit 562 cells (R175H) were treated with indicated concentration of ATO, fixed with or without 0.03% (v/v) glutaraldehyde, followed by p53 immunoblotting.

(F and G), Denaturing (F) and native (G) MS spectra of the purified R249S DBD before or after ATO incubation (1:5 molar ratio).

In (B and C), bars represent mean ± s.d. (n = 3). In (D), representative results from two independent experiments was shown.

See also Figure S2.

Figure 3. Structures of As-Bound p53 Mutants

(A) Cartoon representation of a p53–DNA complex (wild-type DBD, 1TUP chain B). The LSH motif is colored in blue while the L2 and L3 loops are in cyan. The Zn coordinating residues and cysteines in the As-binding site are shown as sticks.

(B and C) Cartoon illustration of an As-bound G245S (chain D) (B) and cut-through of surface representation of an As-bound R249S (chain A) (C) from a perspective equivalent to (A).

(D–F) A close-up of the local structure of L3 loop. (D) An As-bound G245S DBD superposed with wild-type DBD and As-free G245S DBD. The structural water molecule observed for wild-type p53 is displaced by S245. (E) An As-bound R249S DBD superimposed with wild-type DBD and As-free R249S DBD. Zn from wild-type DBD is shown as a sphere. The dashed orange curve indicates a disordered region. (F) An As-bound R249S DBD superimposed with wild-type DBD. The Ser249/Arg249, Glu171 and Arg174 are shown as sticks. Salt bridges are indicated with dashed lines.

See also Figure S3 and Table S4.

Figure 4. The Cryptic As-Binding Pocket

(A and B) The As-coordination site of G245S DBD (A) and R249S DBD (B) with the ABP residues shown as sticks. Electron density ($2F_o{-}F_c$ map, contoured at 2 σ) within a 4-Å radius of the As coordinates and for the side chains of ABP residues and the As atom is illustrated as blue mesh. The covalent S–As bonds are indicated as dashed lines.

(C) Cartoon representation of G245S DBD with the LSH motif colored in green while the rest of the molecule is in grey.

(D) R249S DBD with ABP residues shown as sticks. Electron density ($2F_o{-}F_c$ at 2 σ) for the As and the side chains of the ABP and surrounding hydrophobic residues is illustrated as blue mesh.

(E) Illustration of G245S DBD (left panel) and solvent-accessible surface representation of the ABP (upper right) and the Zn-coordination site (lower right). The side chains of the ABP and the Zn-coordinating residues are shown as sticks, and are omitted from the surface representation for clarity.

(F) An *apo* p53 DBD and a DNA-complexed p53 DBD are superimposed on the As-bound DBD-R249S with ABP residues shown as sticks. Side chain rotations induced by As binding are indicated by arrows.

(G – I) PAb1620 IP assay for the indicated p53 mutants in ATO-treated H1299 cells. In (H), the vertical lines indicated the blots were cut and spliced together.

(J and K) Sequence and structural alignments of p53 homologs. (J) The so-termed conserved region II of p53 homologs is shown with identical residues and the ABP-corresponding residues highlighted. (K) Close-up views of the ABP-equivalent residues from crystal structures of p53 orthologs (left) and paralogs (right).

See also Figure S4.

Figure 5. Transcriptional Reactivation by ATO

(A) Luciferase reporter assay of the indicated six p53 hotspot mutants for the indicated targets upon ATO treatment for 24 h in H1299 cells. Bar graph shows normalized relative luciferase unit (RLU). Immunoblotting shows the relative levels of transfected p53.

(B–E) Luciferase reporter assays for p53-R282W in the indicated contexts. (B) assay of the indicated promoters in the indicated p53-null cell lines. (C) assay of ATO concentration. (D) assay of the indicated p53 mutants. (E) assay of the indicated p53 and p63 mutants.

(F and G) qPCR determination for the mRNA levels (F) and immunoblotting determination for the protein levels (G) of the indicated p53 targets upon ATO treatment. In (F), PATU8988T cell line with relatively high IC_{50} were treated with 2 μg/mL ATO. The others were treated with 1 μg/mL ATO.

In (A)–(F), bars represent mean ± s.d. (n = 3, $^*P < 0.05$).

See also Figure S5.

Figure 6. ATO Rescues Mutant p53 in Tumor Suppression

(A–C) CEM-C1 CDX model. (A) NOD/SCID mice were injected with CEM-C1 cells via tail veins on day 1 and 5 mg/kg ATO was intravenously injected daily from day 23 onwards. (B) PB was harvested on the indicated days, followed by CEM-C1 (human

CD45+) detection by FACS. (C) Mantel–Cox survival curve of the indicated mice. Bars represent mean ± s.d. (*$P < 0.05$).

(D–F) R175H-tet-off H1299 CDX model. (D) Nude mice were subcutaneously injected with R175H-tet-off H1299 cells on day 1 and 5 mg/kg ATO was intraperitoneally injected for 6 consecutive days per week since day 21. In Dox groups, drinking water contained 0.2 mg/mL Dox. (E) Tumor sizes were measured every three days. Immunoblotting shows p53 level in isolated tumors on day 48. (F) Mice were sacrificed on day 48 and isolated tumors weighed. Bars represent mean ± s.e.m. (n = 4 for each group, *$P < 0.05$, **$P < 0.01$, *N.S.*, not significant).

(G–K) NSCLC PDX model. (G) 48 nude mice were subcutaneously implanted with NSCLC tumor tissues on day 1. On day 37, 16 mice with relatively equivalent tumor size were selected and randomly as-signed into 3 groups, followed by intraperitoneal compound administration (PBS, daily injection, n = 8; ATO, 5 mg/kg per injection, daily, n = 4; cisplatin, 5 mg/kg per injection, per week, n = 4). Tumor sizes were measured every 3–4 days. (H) On day 57, all mice were sacrificed and isolated tumors weighed. (I) immunoblotting for the indicated protein in freshly isolated tumors. (J) Immunohistochemistry staining for the isolated tumors. Representative scopes were shown. Scale bar, 50 μm. (K) Percentages of positive cells counted from (J). Each dot in the plot represents sum of the positive cells counted from 3 scopes randomly picked. Each scope includes at least 300 cells. Bars represent mean ± s.d. (*N.S.*, not significant).

See also Figure S6.

Figure 7. Applicable Spectrum of p53 Mutations

(A) Information of the 25 most frequent p53 missense mutations compiled from IARC.

(B and C) PAb1620 IP assay (B) and luciferase reporter assay (C) in H1299 cells transfected with the indicated 25 p53 mutants.

(D and E) Cell viability assay for the indicated cell lines upon ATO treatment for 72 h. In right panel of (D), dots represent the calculated IC_{50}. In (E), mutant p53 in the indicated three cell lines were knocked down by siRNA, followed by cell viability assay.

(F–H) Responses of p53 targets in ATO-treated cell lines. (F) CHIP-qPCR determination for the percentage of DNA bound to mutant p53. The percentages for ATO-untreated samples were normalized as 1. IgG was used as control. (G and H) qPCR determination for the mRNA levels (G) and immunoblotting determination for the protein levels (H) of the indicated p53 targets upon ATO treatment for 24 h and 48 h, respectively. In (F) and (G), the ATO-sensitive line Loucy was treated with 0.04 μg/mL ATO while the other two lines were treated with 1 μg/mL ATO.

(I) p53-null HCT116 cells were introduced with the indicated p53 mutants, followed by ATO treatment for 24 h and RNA sequencing. Heat map showing gene expression (FPKM values) for the reported 116 p53 targets.

(J) The log-log plot showing ATO rescue spectrum derived from the (B) and (C).

(K) The 25 most frequent p53 mutations (mutated residues shown as sticks) are mapped onto a p53–DNA complex (PDB: 1TUP), and colored according to ATO-mediated rescue.

In (C) and (E)–(G), bars represent mean ± s.d. (n = 3, $^{*}P < 0.05$). Box plot in (D) represents a five-number summary: minima, lower quartile, median, upper quartile and maxima.

See also Figure S7 and Table S5.

REFERENCES

Boeckler, F. M., Joerger, A. C., Jaggi, G., Rutherford, T. J., Veprintsev, D. B., and Fersht, A. R. (2008). Targeted rescue of a destabilized mutant of p53 by an in silico screened drug. Proceedings of the National Academy of Sciences of the United States of America *105*, 10360-10365.

Bullock, A. N., and Fersht, A. R. (2001). Rescuing the function of mutant p53. Nature reviews Cancer *1*, 68-76.

Bullock, A. N., Henckel, J., and Fersht, A. R. (2000). Quantitative analysis of residual folding and DNA binding in mutant p53 core domain: definition of mutant states for rescue in cancer therapy. Oncogene *19*, 1245-1256.

Bykov, V. J., Issaeva, N., Shilov, A., Hultcrantz, M., Pugacheva, E., Chumakov, P., Bergman, J., Wiman, K. G., and Selivanova, G. (2002). Restoration of the tumor suppressor function to mutant p53 by a low-molecular-weight compound. Nature medicine *8*, 282-288.

Bykov, V. J., Zache, N., Stridh, H., Westman, J., Bergman, J., Selivanova, G., and Wiman, K. G. (2005). PRIMA-1(MET) synergizes with cisplatin to induce tumor cell apoptosis. Oncogene *24*, 3484-3491.

Chen, G. Q., Shi, X. G., Tang, W., Xiong, S. M., Zhu, J., Cai, X., Han, Z. G., Ni, J. H., Shi, G. Y., Jia, P. M., *et al.* (1997). Use of arsenic trioxide (As2O3) in the treatment of acute promyelocytic leukemia (APL): I. As2O3 exerts dose-dependent dual effects on APL cells. Blood *89*, 3345-3353.

Chen, G. Q., Zhu, J., Shi, X. G., Ni, J. H., Zhong, H. J., Si, G. Y., Jin, X. L., Tang, W., Li, X. S., Xong, S. M., *et al.* (1996). In vitro studies on cellular and molecular mechanisms of arsenic trioxide (As2O3) in the treatment of acute promyelocytic leukemia: As2O3 induces NB4 cell apoptosis with downregulation of Bcl-2 expression and modulation of PML-RAR alpha/PML proteins. Blood *88*, 1052-1061.

Chen, S., Bubeck, D., MacDonald, B. T., Liang, W. X., Mao, J. H., Malinauskas, T., Llorca, O., Aricescu, A. R., Siebold, C., He, X., and Jones, E. Y. (2011). Structural and Functional Studies of LRP6 Ectodomain Reveal a Platform for Wnt Signaling. Dev Cell *21*, 848-861.

Chen, S., Wu, J., Zhong, S., Li, Y., Zhang, P., Ma, J., Ren, J., Tan, Y., Wang, Y., Au, K. F., *et al.* (2019). iASPP mediates p53 selectivity through a modular mechanism fine-tuning DNA recognition. Proceedings of the National Academy of Sciences of the United States of America *116*, 17470-17479.

Cho, Y., Gorina, S., Jeffrey, P. D., and Pavletich, N. P. (1994). Crystal structure of a p53 tumor suppressor-DNA complex: understanding tumorigenic mutations. Science *265*, 346-355.

de The, H., Pandolfi, P. P., and Chen, Z. (2017). Acute Promyelocytic Leukemia: A Paradigm for Oncoprotein-Targeted Cure. Cancer Cell *32*, 552-560.

Dobin, A., Davis, C. A., Schlesinger, F., Drenkow, J., Zaleski, C., Jha, S., Batut, P., Chaisson, M., and Gingeras, T. R. (2013). STAR: ultrafast universal RNA-seq aligner. Bioinformatics *29*, 15-21.

Emsley, P., and Cowtan, K. (2004). Coot: model-building tools for molecular graphics. Acta Crystallogr D Biol Crystallogr *60*, 2126-2132.

Fischer, M. (2017). Census and evaluation of p53 target genes. Oncogene *36*, 3943-3956.

Friedman, P. N., Chen, X., Bargonetti, J., and Prives, C. (1993). The p53 protein is an unusually shaped tetramer that binds directly to DNA. Proceedings of the National Academy of Sciences of the United States of America *90*, 3319-3323.

Gannon, J. V., Greaves, R., Iggo, R., and Lane, D. P. (1990). Activating mutations in p53 produce a common conformational effect. A monoclonal antibody specific for the mutant form. The EMBO journal *9*, 1595-1602.

Hu, J., Liu, Y. F., Wu, C. F., Xu, F., Shen, Z. X., Zhu, Y. M., Li, J. M., Tang, W., Zhao, W. L., Wu, W., *et al.* (2009). Long-term efficacy and safety of all-trans retinoic acid/arsenic trioxide-based therapy in newly diagnosed acute promyelocytic leukemia. Proceedings of the National Academy of Sciences of the United States of America *106*, 3342-3347.

Hu, X., Cai, J., Zhu, J., Lang, W., Zhong, J., Zhong, H., and Chen, F. (2020). Arsenic trioxide potentiates Gilteritinib-induced apoptosis in FLT3-ITD positive leukemic cells via IRE1a-JNK-mediated endoplasmic reticulum stress. Cancer Cell Int *20*, 250.

Hughes, M. F., Kenyon, E. M., Edwards, B. C., Mitchell, C. T., and Thomas, D. J. (1999). Strain-dependent disposition of inorganic arsenic in the mouse. Toxicology *137*, 95-108.

Jing, Y., Wang, L., Xia, L., Chen, G. Q., Chen, Z., Miller, W. H., and Waxman, S. (2001). Combined effect of all-trans retinoic acid and arsenic trioxide in acute promyelocytic leukemia cells in vitro and in vivo. Blood *97*, 264-269.

Joerger, A. C., Ang, H. C., and Fersht, A. R. (2006). Structural basis for understanding oncogenic p53 mutations and designing rescue drugs. Proceedings of the National Academy of Sciences of the United States of America *103*, 15056-15061.

Joerger, A. C., and Fersht, A. R. (2008). Structural biology of the tumor suppressor p53. Annual review of biochemistry *77*, 557-582.

Joerger, A. C., and Fersht, A. R. (2010). The tumor suppressor p53: from structures to drug discovery. Cold Spring Harb Perspect Biol *2*, a000919.

Joerger, A. C., and Fersht, A. R. (2016). The p53 Pathway: Origins, Inactivation in Cancer, and Emerging Therapeutic Approaches. Annual review of biochemistry *85*, 375-404.

Kabsch, W. J. A. C. S. D. B. C. (2010). Xds. *66*, 125-132.

Kandoth, C., McLellan, M. D., Vandin, F., Ye, K., Niu, B., Lu, C., Xie, M., Zhang, Q., McMichael, J. F., Wyczalkowski, M. A., *et al.* (2013). Mutational landscape and significance across 12 major cancer types. Nature *502*, 333-339.

Kitchin, K. T., and Wallace, K. (2006). Dissociation of arsenite-peptide complexes: triphasic nature, rate constants, half-lives, and biological importance. Journal of biochemical and molecular toxicology *20*, 48-56.

Krissinel, E., and Henrick, K. (2004). Secondary-structure matching (SSM), a new tool for fast protein structure alignment in three dimensions. Acta Crystallogr D Biol Crystallogr *60*, 2256-2268.

Lallemand-Breitenbach, V., Guillemin, M. C., Janin, A., Daniel, M. T., Degos, L., Kogan, S. C., Bishop, J. M., and de The, H. (1999). Retinoic acid and arsenic synergize to eradicate leukemic cells in a mouse model of acute promyelocytic leukemia. The Journal of experimental medicine *189*, 1043-1052.

Levine, A. J. (2019). Targeting Therapies for the p53 Protein in Cancer Treatments. Annual Review of Cancer Biology *3*, 21-34.

Liu, Q., Hilsenbeck, S., and Gazitt, Y. (2003). Arsenic trioxide-induced apoptosis in myeloma cells: p53-dependent G1 or G2/M cell cycle arrest, activation of caspase-8 or caspase-9, and synergy with APO2/TRAIL. Blood *101*, 4078-4087.

Lu, M., Breyssens, H., Salter, V., Zhong, S., Hu, Y., Baer, C., Ratnayaka, I., Sullivan, A., Brown, N. R., Endicott, J., *et al.* (2013). Restoring p53 function in human melanoma cells by inhibiting MDM2 and cyclin B1/CDK1-phosphorylated nuclear iASPP. Cancer cell *23*, 618-633.

Martin, M. (2011). Cutadapt removes adapter sequences from high-throughput sequencing reads. 2011 *17*, 3 %J EMBnet.journal.

McCoy, A. J., Grosse-Kunstleve, R. W., Adams, P. D., Winn, M. D., Storoni, L. C., and Read, R. J. (2007a). Phaser crystallographic software. J Appl Crystallogr *40*, 658-674.

McCoy, A. J., Grosse-Kunstleve, R. W., Adams, P. D., Winn, M. D., Storoni, L. C., and Read, R. J. J. J. o. a. c. (2007b). Phaser crystallographic software. *40*, 658-674.

Modi, M., Pathak, U., Kalia, K., and Flora, S. J. (2005). Arsenic antagonism studies with monoisoamyl DMSA and zinc in male mice. Environmental toxicology and pharmacology *19*, 131-138.

Nikolova, P. V., Henckel, J., Lane, D. P., and Fersht, A. R. (1998). Semirational design of active tumor suppressor p53 DNA binding domain with enhanced stability. Proceedings of the National Academy of Sciences of the United States of America *95*, 14675-14680.

Olivier, M., Hollstein, M., and Hainaut, P. (2010). TP53 mutations in human cancers: origins, consequences, and clinical use. Cold Spring Harb Perspect Biol *2*, a001008.

Petty, T. J., Emamzadah, S., Costantino, L., Petkova, I., Stavridi, E. S., Saven, J. G., Vauthey, E., and Halazonetis, T. D. (2011). An induced fit mechanism regulates p53 DNA binding kinetics to confer sequence specificity. EMBO J *30*, 2167-2176.

Reinhold, W. C., Sunshine, M., Liu, H., Varma, S., Kohn, K. W., Morris, J., Doroshow, J., and Pommier, Y. (2012). CellMiner: a web-based suite of genomic and pharmacologic tools to explore transcript and drug patterns in the NCI-60 cell line set. Cancer research *72*, 3499-3511.

Schneider, C. A., Rasband, W. S., and Eliceiri, K. W. (2012). NIH Image to ImageJ: 25 years of image analysis. Nat Methods *9*, 671-675.

Shoemaker, R. H. (2006). The NCI60 human tumour cell line anticancer drug screen. Nature reviews Cancer *6*, 813-823.

Suad, O., Rozenberg, H., Brosh, R., Diskin-Posner, Y., Kessler, N., Shimon, L. J., Frolow, F., Liran, A., Rotter, V., and Shakked, Z. (2009). Structural basis of restoring sequence-specific DNA binding and transactivation to mutant p53 by suppressor mutations. Journal of molecular biology *385*, 249-265.

Vagin, A. A., Steiner, R. A., Lebedev, A. A., Potterton, L., McNicholas, S., Long, F., and Murshudov, G. N. J. A. C. S. D. B. C. (2004). REFMAC5 dictionary: organization of prior chemical knowledge and guidelines for its use. *60*, 2184-2195.

Vassilev, L. T., Vu, B. T., Graves, B., Carvajal, D., Podlaski, F., Filipovic, Z., Kong, N., Kammlott, U., Lukacs, C., Klein, C., *et al.* (2004). In vivo activation of the p53 pathway by small-molecule antagonists of MDM2. Science *303*, 844-848.

Wang, H., Liu, Y., Wang, X., Liu, D., Sun, Z., Wang, C., Jin, G., Zhang, B., and Yu, S. (2015). Randomized clinical control study of locoregional therapy combined with arsenic trioxide for the treatment of hepatocellular carcinoma. Cancer *121*, 2917-2925.

Wang, L., Liang, W., Peng, N., Hu, X., Xu, Y., and Liu, Z. (2017). The synergistic antitumor effect of arsenic trioxide combined with cytotoxic T cells in pulmonary metastasis model of colon cancer. Oncotarget *8*, 109609-109618.

Wang, P. L., Sait, F., and Winter, G. (2001). The 'wildtype' conformation of p53: epitope mapping using hybrid proteins. Oncogene *20*, 2318-2324.

Wang, R., Xia, L., Gabrilove, J., Waxman, S., and Jing, Y. (2013). Downregulation of Mcl-1 through GSK-3beta activation contributes to arsenic trioxide-induced apoptosis in acute myeloid leukemia cells. Leukemia *27*, 315-324.

Wang, Z. Y., and Chen, Z. (2008). Acute promyelocytic leukemia: from highly fatal to highly curable. Blood *111*, 2505-2515.

Wilcken, R., Wang, G., Boeckler, F. M., and Fersht, A. R. (2012). Kinetic mechanism of p53 oncogenic mutant aggregation and its inhibition. Proceedings of the National Academy of Sciences of the United States of America *109*, 13584-13589.

Williams, C. J., Headd, J. J., Moriarty, N. W., Prisant, M. G., Videau, L. L., Deis, L. N., Verma, V., Keedy, D. A., Hintze, B. J., Chen, V. B., *et al.* (2018). MolProbity: More and better reference data for improved all-atom structure validation. Protein Sci *27*, 293-315.

Wong, K. B., DeDecker, B. S., Freund, S. M., Proctor, M. R., Bycroft, M., and Fersht, A. R. (1999). Hot-spot mutants of p53 core domain evince characteristic local structural changes. Proc Natl Acad Sci U S A *96*, 8438-8442.

Yan, W., Jung, Y. S., Zhang, Y., and Chen, X. (2014). Arsenic trioxide reactivates proteasome-dependent degradation of mutant p53 protein in cancer cells in part via enhanced expression of Pirh2 E3 ligase. Plos One *9*, e103497.

Yan, W., Zhang, Y., Zhang, J., Liu, S., Cho, S. J., and Chen, X. (2011). Mutant p53 protein is targeted by arsenic for degradation and plays a role in arsenic-mediated growth suppression. The Journal of biological chemistry *286*, 17478-17486.

Yap, D. B., Hsieh, J. K., Zhong, S., Heath, V., Gusterson, B., Crook, T., and Lu, X. (2004). Ser392 phosphorylation regulates the oncogenic function of mutant p53. Cancer research *64*, 4749-4754.

Yu, X., Vazquez, A., Levine, A. J., and Carpizo, D. R. (2012). Allele-specific p53 mutant reactivation. Cancer cell *21*, 614-625.

Zehir, A., Benayed, R., Shah, R. H., Syed, A., Middha, S., Kim, H. R., Srinivasan, P., Gao, J., Chakravarty, D., Devlin, S. M., *et al.* (2017). Mutational landscape of metastatic cancer revealed from prospective clinical sequencing of 10,000 patients. Nat Med *23*, 703-713.

Zhang, Q., Bykov, V. J. N., Wiman, K. G., and Zawacka-Pankau, J. (2018). APR-246 reactivates mutant p53 by targeting cysteines 124 and 277. Cell death & disease *9*, 439.

Zhang, X. W., Yan, X. J., Zhou, Z. R., Yang, F. F., Wu, Z. Y., Sun, H. B., Liang, W. X., Song, A. X., Lallemand-Breitenbach, V., Jeanne, M., *et al.* (2010). Arsenic trioxide controls the fate of the PML-RARalpha oncoprotein by directly binding PML. Science *328*, 240-243.

Zhu, H. H., Wu, D. P., Jin, J., Li, J. Y., Ma, J., Wang, J. X., Jiang, H., Chen, S. J., and Huang, X. J. (2013). Oral tetra-arsenic tetra-sulfide formula versus intravenous arsenic trioxide as first-line treatment of acute promyelocytic leukemia: a multicenter randomized controlled trial. Journal of clinical oncology : official journal of the American Society of Clinical Oncology *31*, 4215-4221.

Figure 1

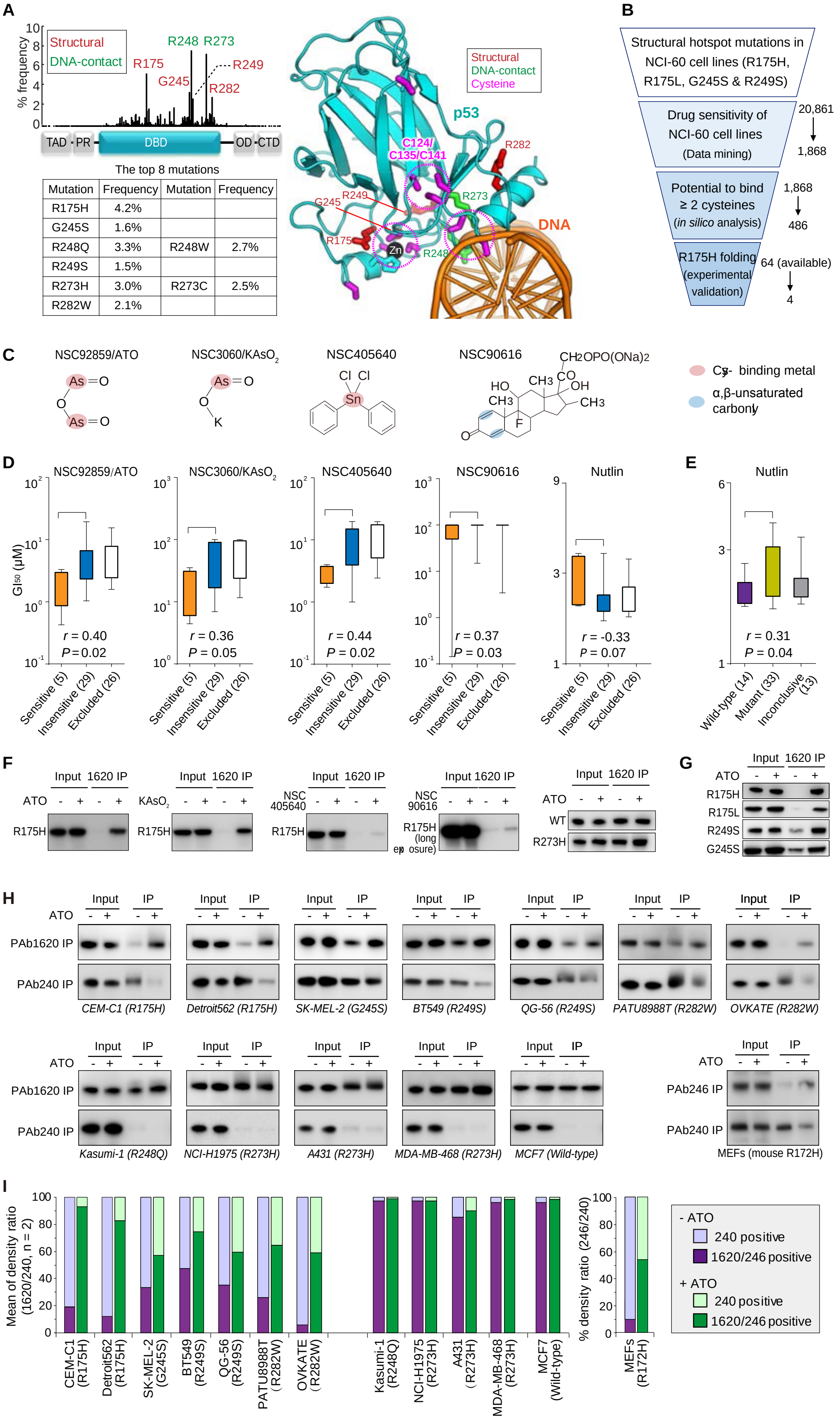

The top 8 mutations

Mutation	Frequency	Mutation	Frequency
R175H	4.2%		
G245S	1.6%		
R248Q	3.3%	R248W	2.7%
R249S	1.5%		
R273H	3.0%	R273C	2.5%
R282W	2.1%		

Figure 1

Figure 2

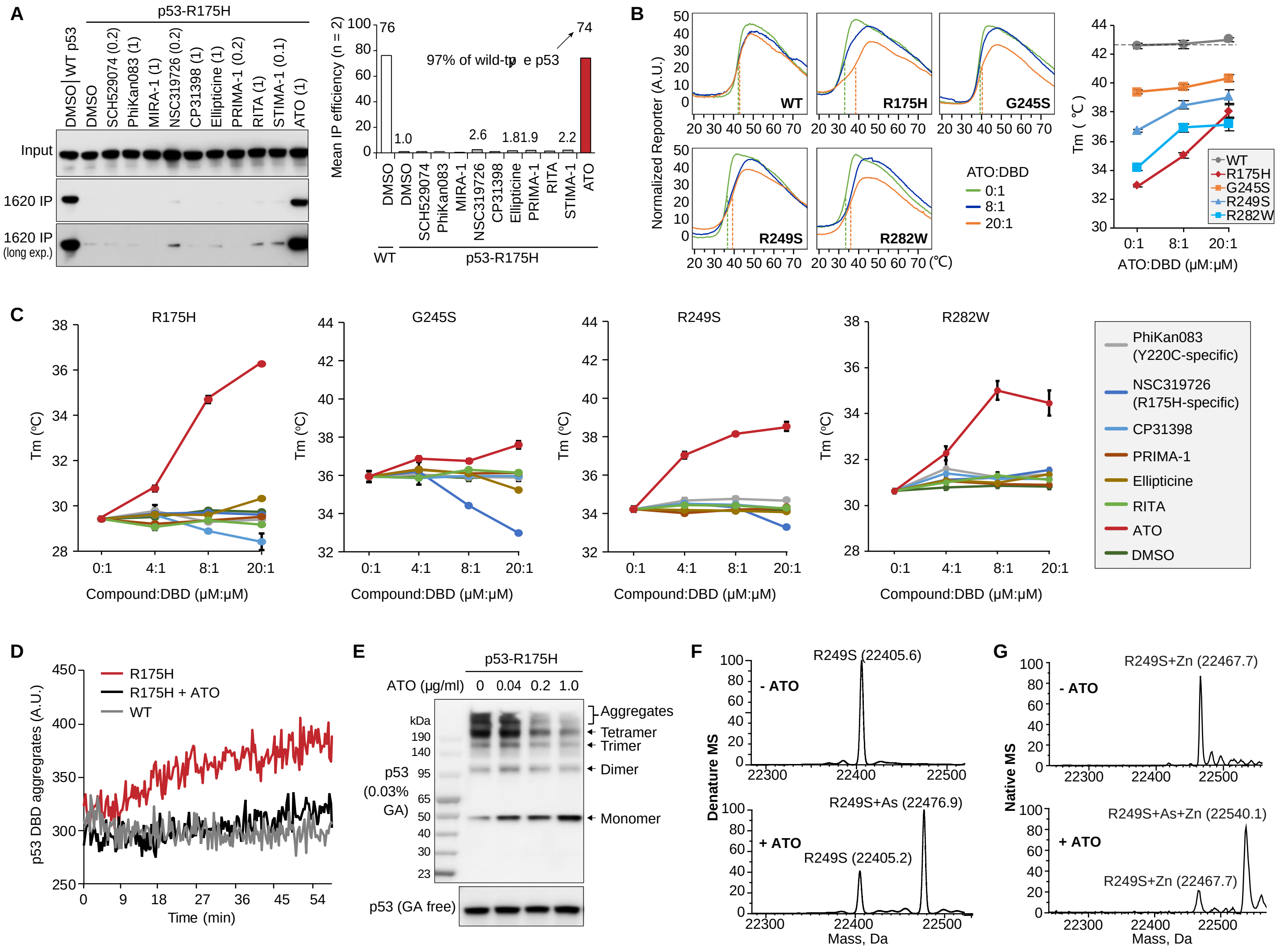

Figure 2

Figure 3

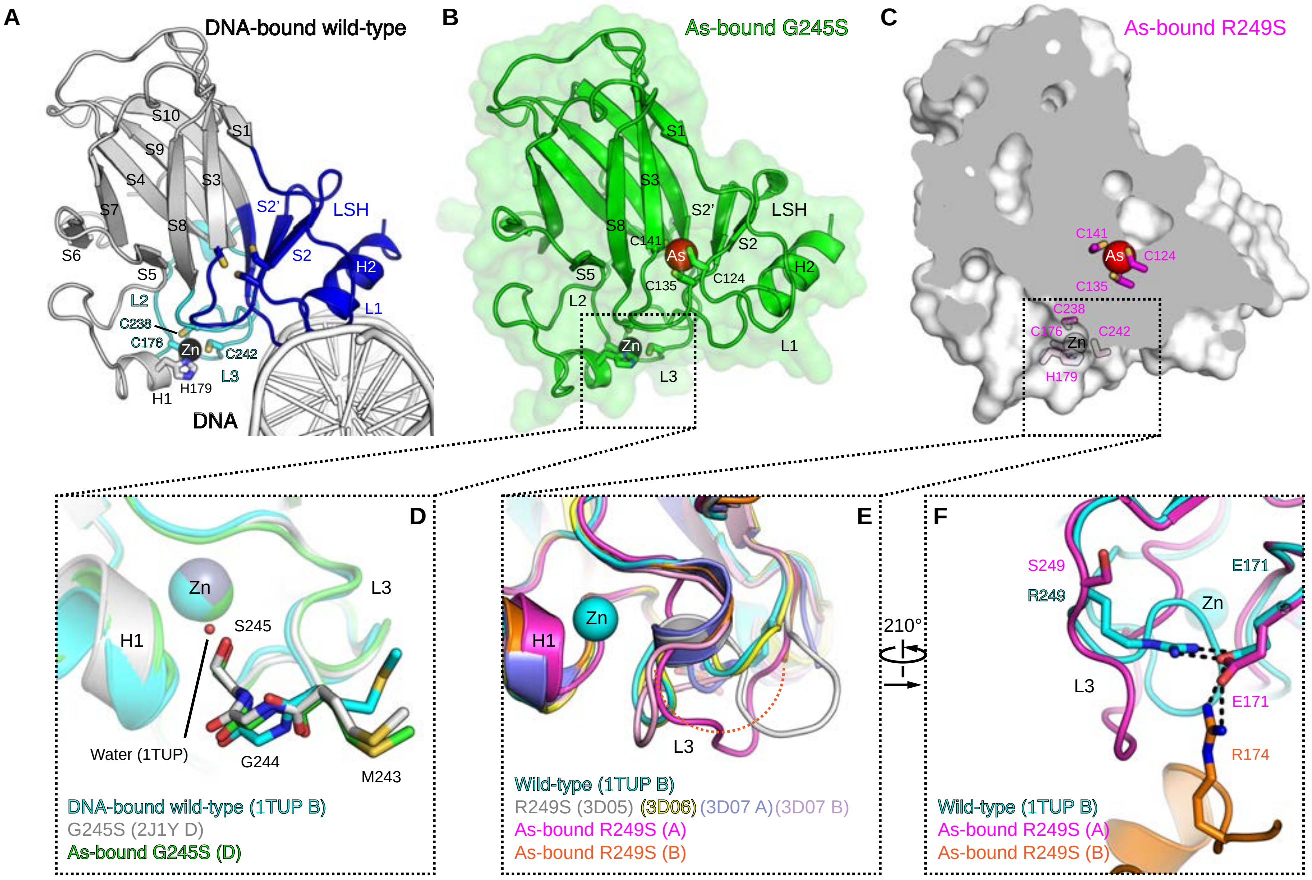

Figure 3

Figure 4

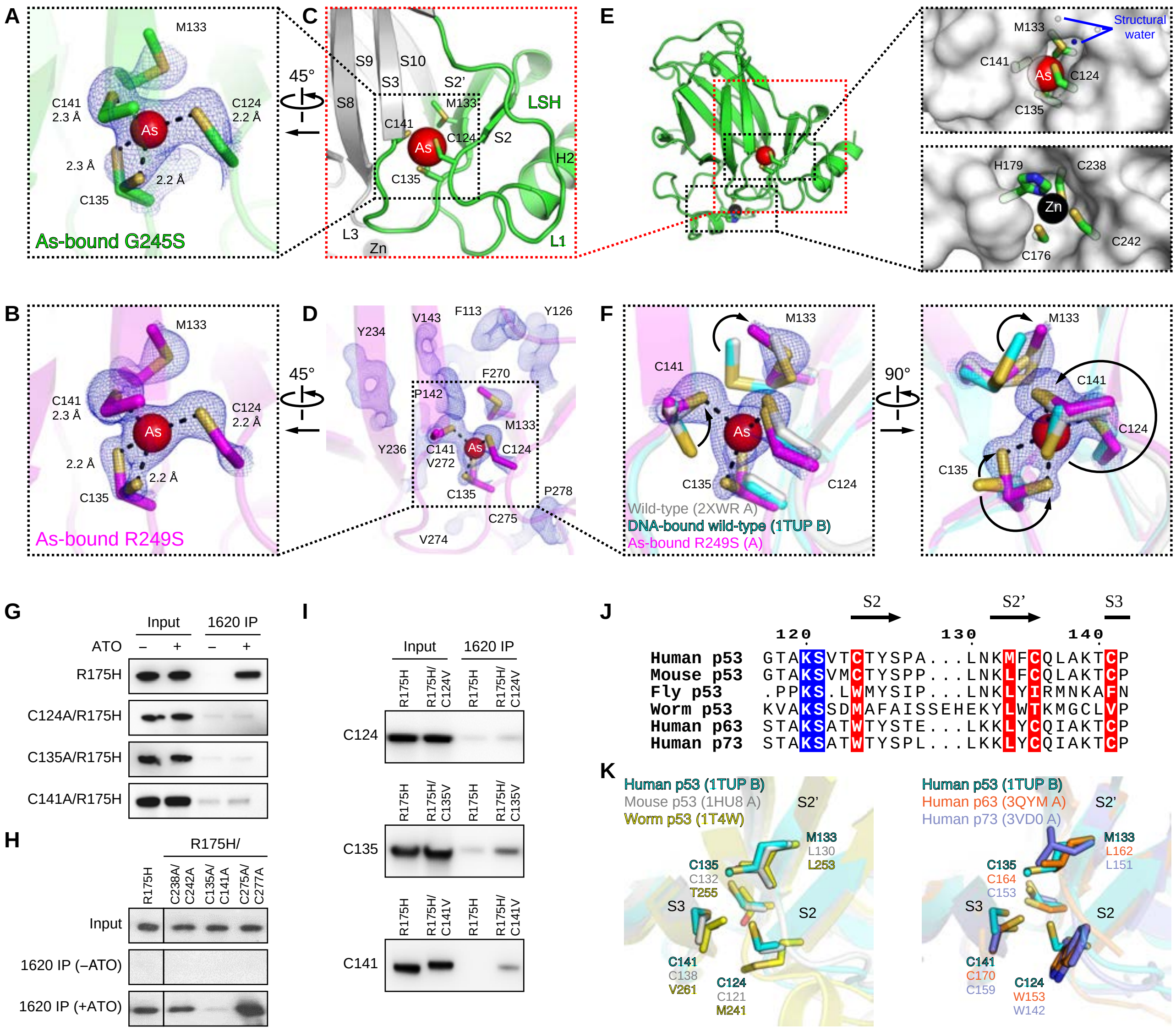

Figure 4

Figure 5

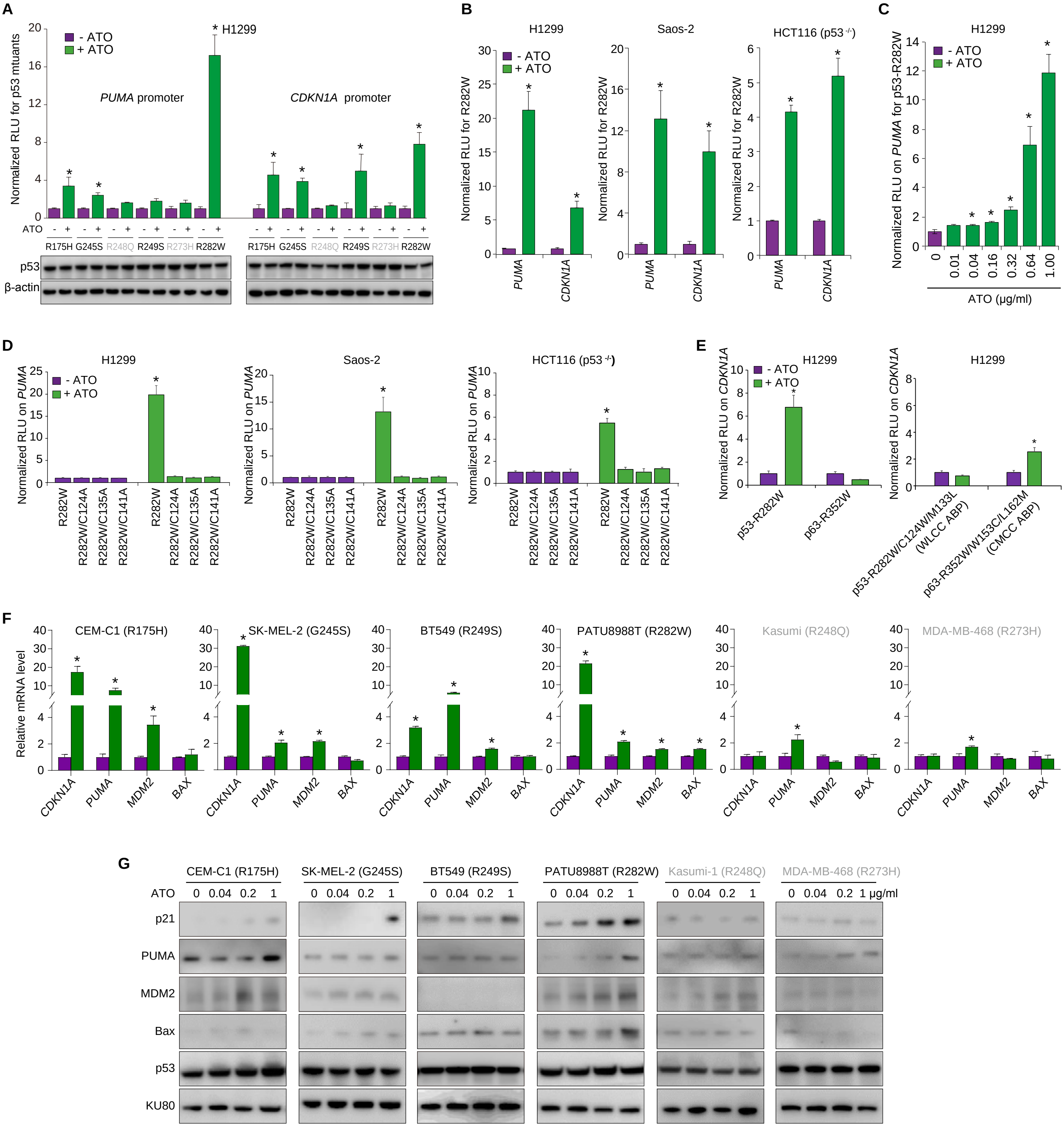

Figure 5

Figure 6

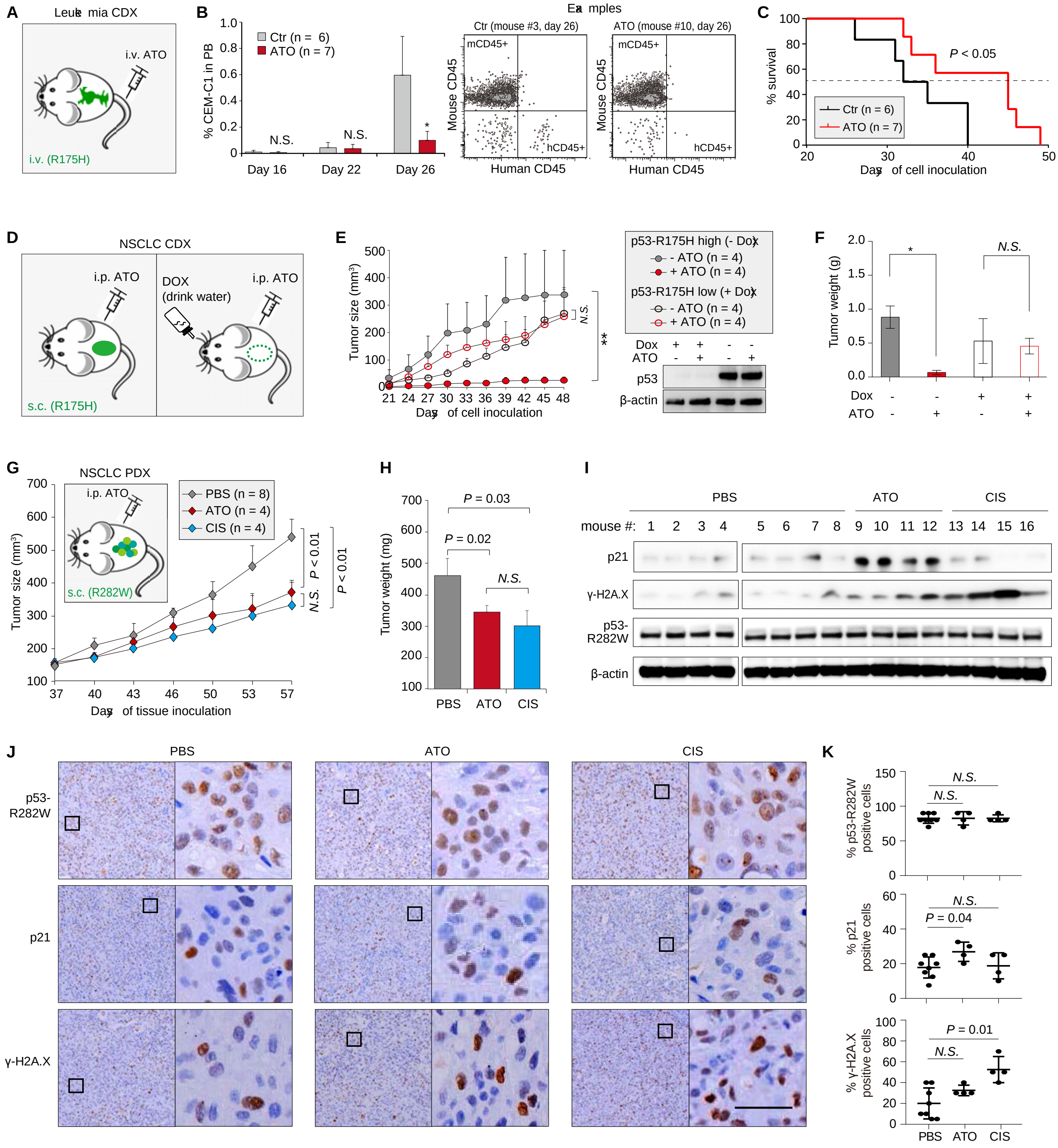

Figure 6

Figure 7

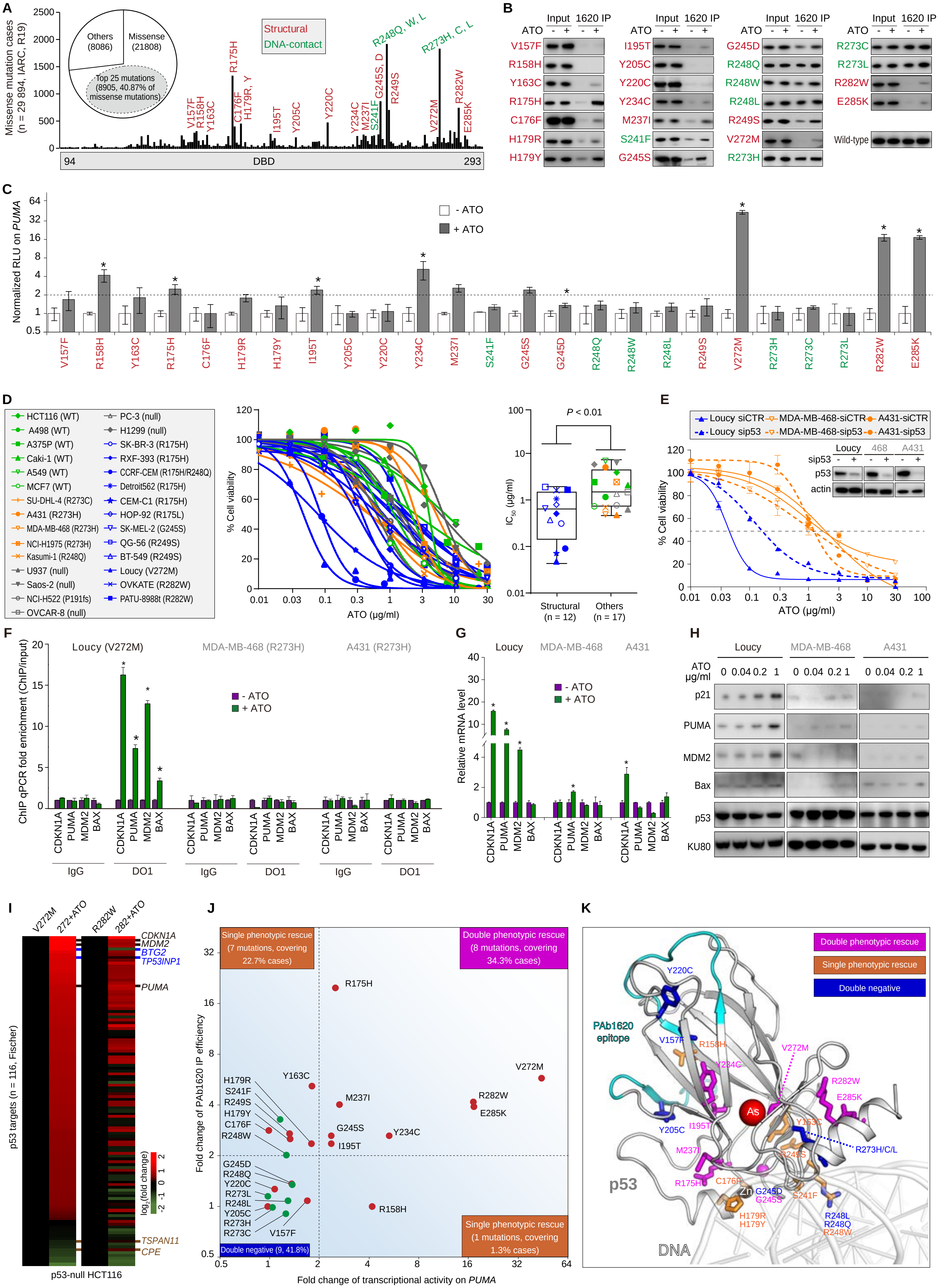

Figure 7

Supplemental Information

Table S4. Crystallographic Refinement, Related to Figure 3.

	As-bound G245S	As-bound R249S
Data collection		
Space group	P 1 21 1	P 1 21 1
Cell dimensions		
a, b, c (Å)	68.11, 68.24, 83.62	41.55, 68.77, 66.78
α, β, γ (°)	90.00, 90.03, 90.00	90.00, 93.22, 90.00
Resolution (Å)	50.00 – 2.15 (2.22 – 2.15)	50.00 - 1.75 (1.81-1.75)
R_{merge}	0.083 (0.260)	0.095 (0.490)
I / σI	12.7 (6.6)	11.1 (2.1)
Completeness (%)	94.8% (93.3%)	94.3% (94.3%)
Redundancy	4.2 (6.6)	2.5 (2.4)
Refinement		
Resolution (Å)	48.21 – 2.15	41.52 - 1.74
No. reflections	37578	34189
R_{work} / R_{free}	0.187/0.219	0.197/0.257
No. atoms		
Protein	6151	3022
As^{3+}	4	2
Zn^{2+}	4	2
SO_4^{2-}	5	-
Water	517	462
GOL	42	18
B-factors(Å^2)		
Protein	37.52	20.39
As^{3+}	46.02	38.53
Zn^{2+}	53.6	21.41
SO_4^{2-}	38.67	-
Water	36.22	28.22
GOL	48.64	43.19
R.m.s. deviations		
Bond lengths (Å)	0.009	0.01
Bond angles (°)	1.304	1.39

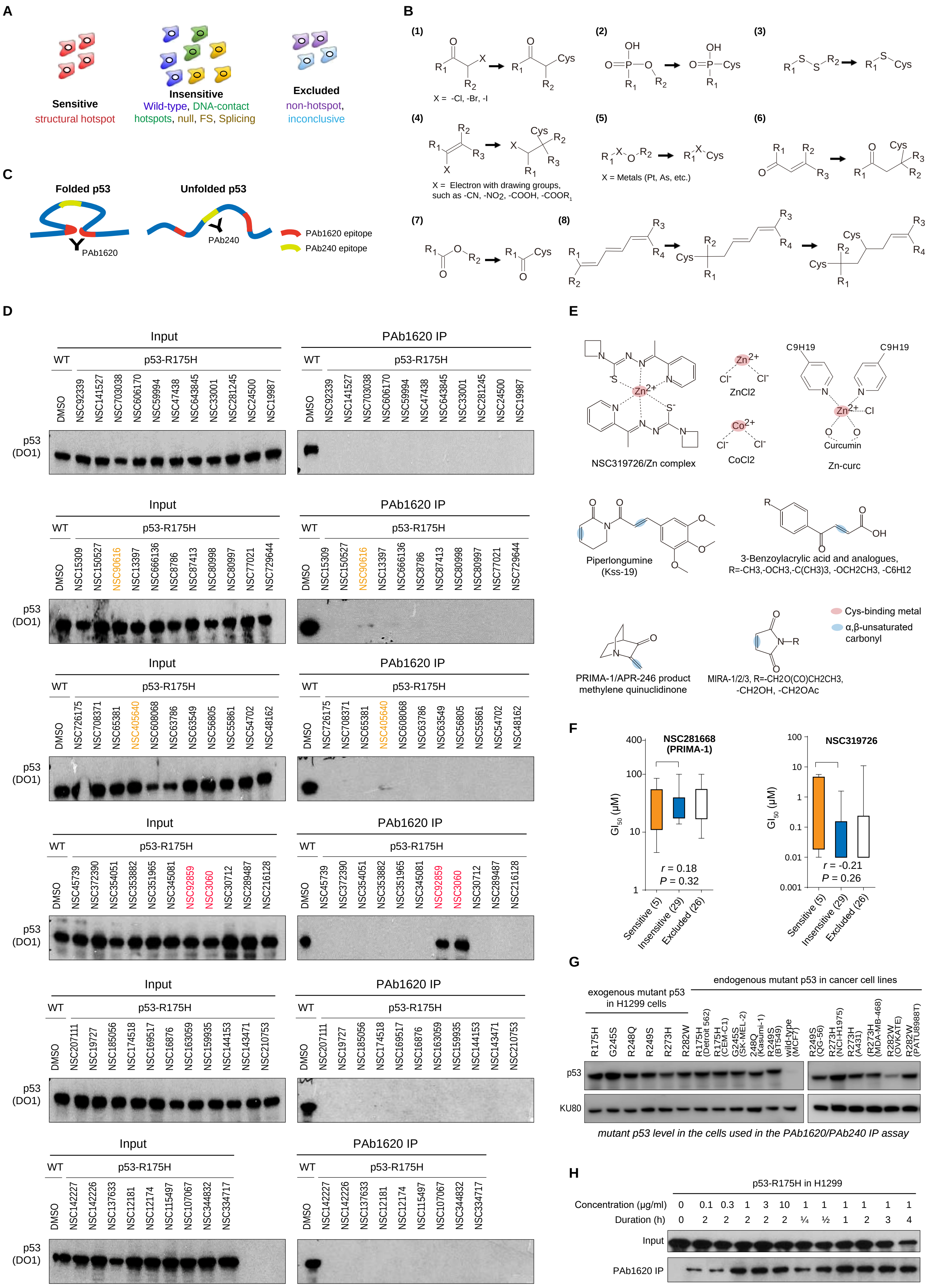

(legend on next page)

Figure S1. Identification of arsenic compounds, Related to Figure 1.

(**A**) NCI-60 cell lines were classified into three groups according to their p53 status. See STAR Methods for details.

(**B**) The eight substructures predicted to bind cysteine.

(**C**) Cartoon scheme representing the locations of PAb1620 and PAb240 epitopes in p53.

(**D**) PAb1620 IP result for the indicated 64 compounds.

(**E**) Chemical structure of the reported mutant p53 rescue compounds.

(**F**) Plot graphs of the GI50 of PRIMA-1 and NSC319726 on the NCI-60 cell lines.

(**G**) Protein level of exogenous (Figure 1F) and endogenous (Figure 1H) p53 in the whole-cell lysate determined by immunoblotting.

(**H**) H1299 cells expressing p53-R175H were treated with ATO under the indicated conditions, followed by PAb1620 IP.

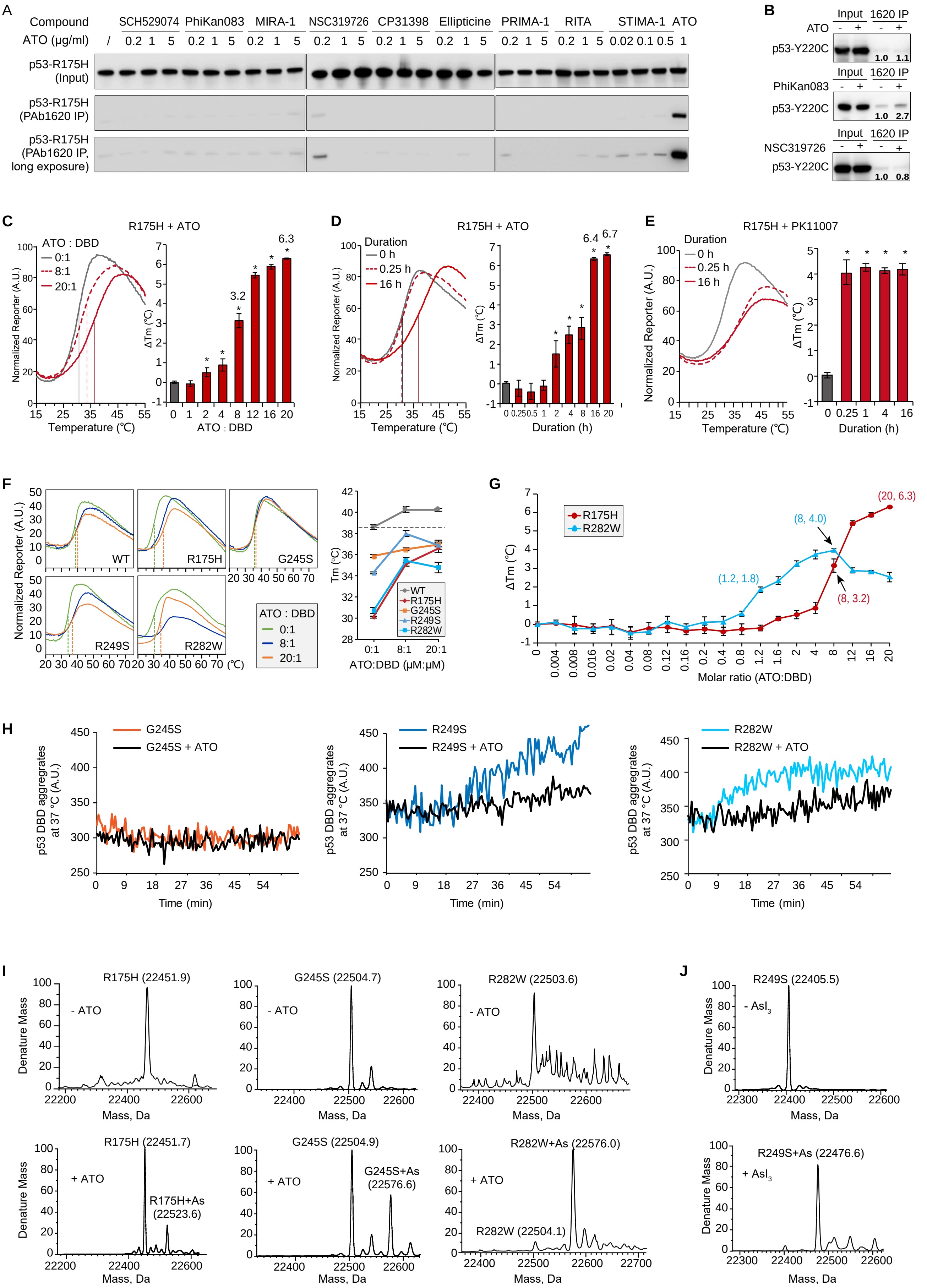

(legend on next page)

Figure S2. ATO stabilizes p53 by covalent binding, Related to Figure 2.

(**A**) H1299 cells expressing p53-R175H were treated with indicated agents at indicated concentrations, followed by PAb1620 IP.

(**B**) H1299 cells expressing p53-Y220C were treated with ATO, PhiKan083, or NSC319726 (1, 1, and 0.2 μg/mL, respectively) overnight, followed by PAb1620 IP assay.

(**C**–**E**) Tm determination for recombinant R175H DBD in the indicated contexts. (C) Determination for ATO: DBD incubation ratios overnight. (D and E) Determination for ATO and PK11007 incubation duration at 1:20 ratio.

(**F**) Assays as in Figure 2B. Salt-free HEPES buffer was used.

(**G**) R175H or R282W DBD was mixed with ATO at the indicated ratios in HEPES buffer overnight. Graph shows the calculated change of Tm (ΔTm).

(**H**) Assays as in Figure 2D.

(**I** and **J**) Denaturing MS spectra of the indicated p53 DBD before or after treatment of the indicated compounds (1:5 molar ratio).In (C)–(G), bars represent mean ± s.d. (n = 3).

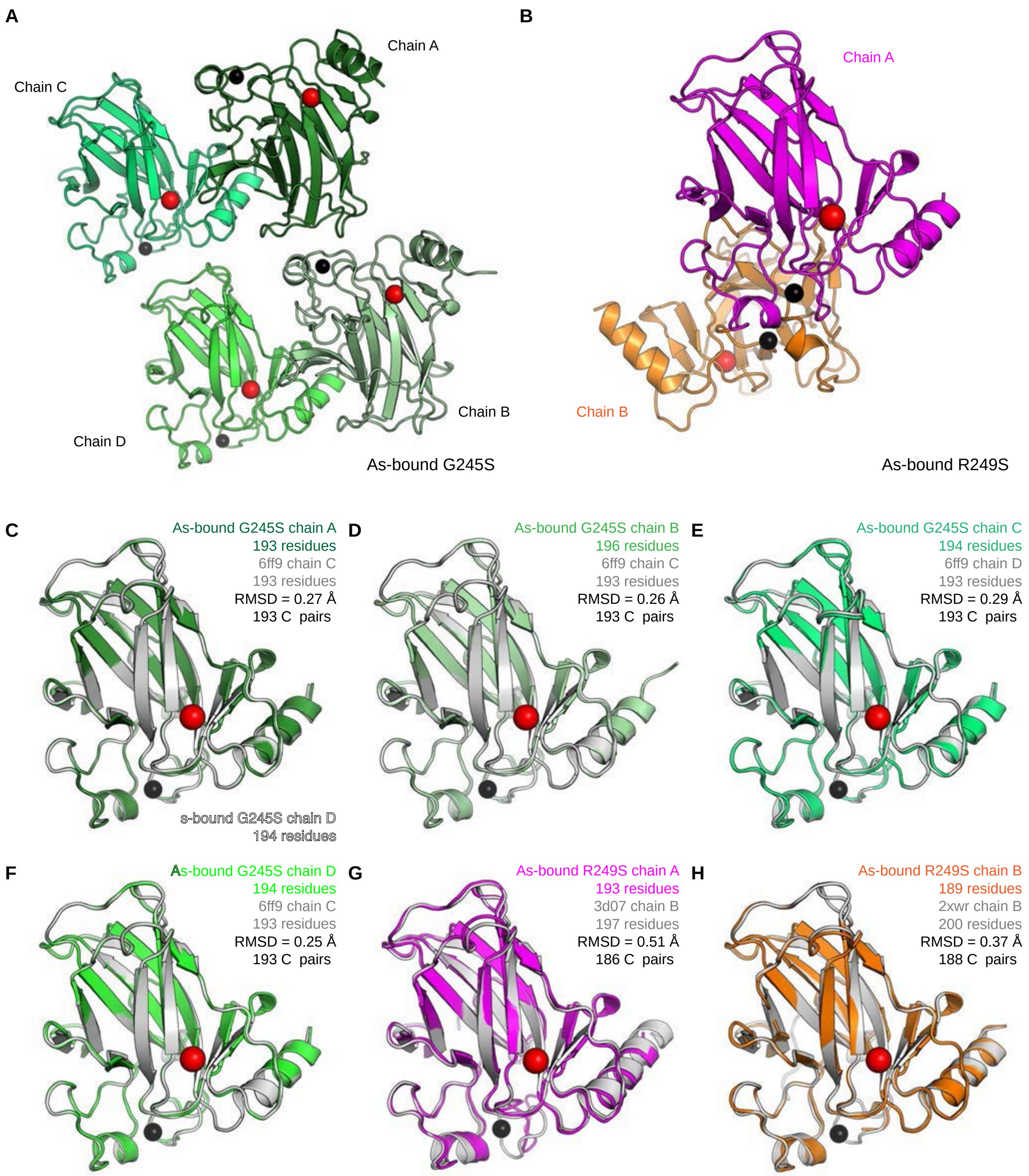

Figure S3. Crystal Structures of As-Bound p53 DBD Mutants, Related to Figure 3.
(**A** and **B**) Crystallographic asymmetrical units of As-bound G245S DBD (A, four DBD copies) and As-bound R249S DBD (B, two DBD copies). In both panels, As atoms are shown as red spheres while Zn atoms as black spheres.
(**C**–**H**) Structural alignment of each of the As-bound mutant p53 DBD molecules with the respective best matched DBD in the database.

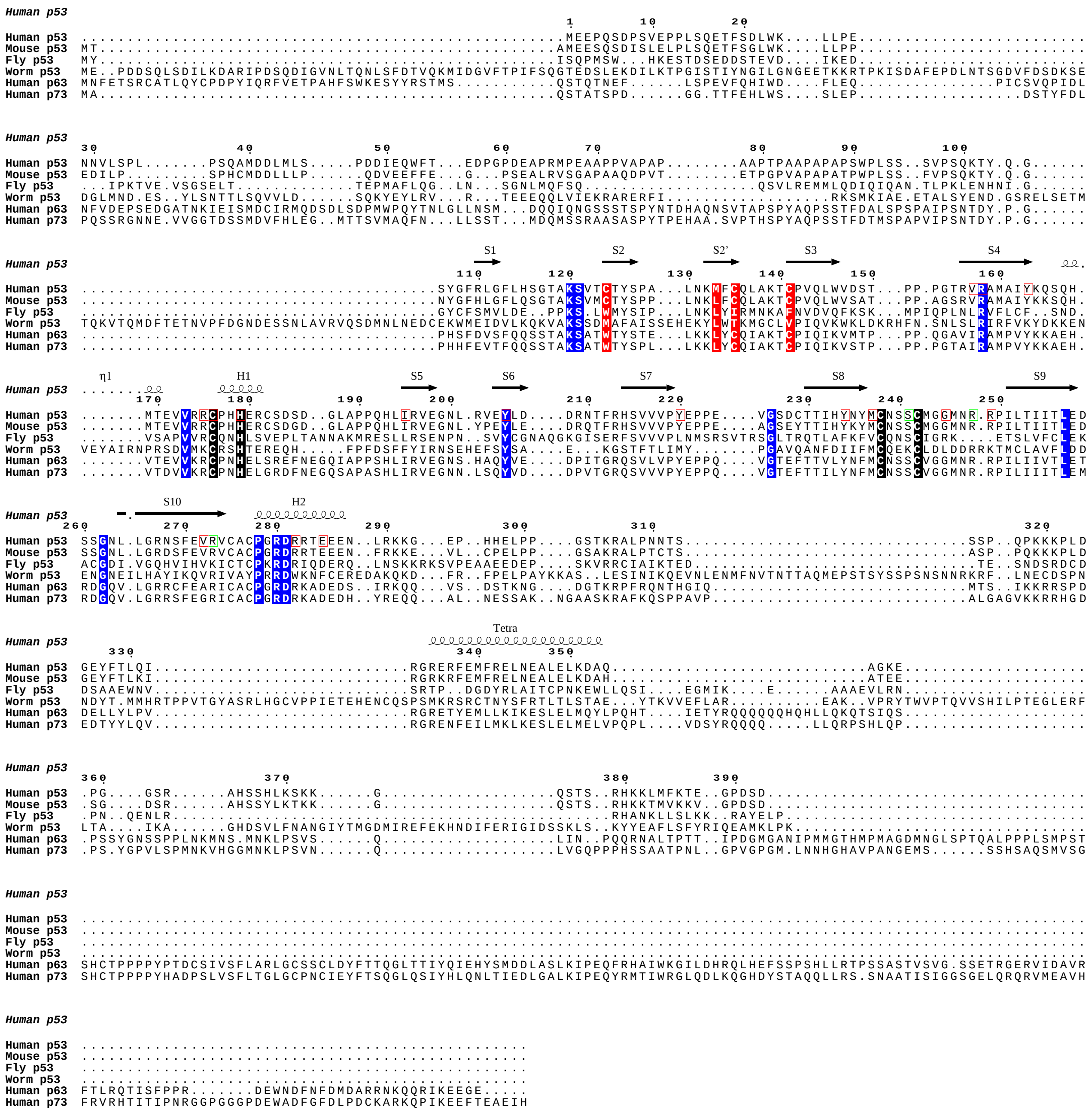

```
Human p53
                                                      1        10        20
Human p53  .....................................................MEEPQSDPSVEPPLSQETFSDLWK....LLPE.........................
Mouse p53  MT..................................................AMEESQSDISLELPLSQETFSGLWK....LLPP.........................
Fly p53    MY..................................................ISQPMSW...HKESTDSEDDSTEVD....IKED.........................
Worm p53   ME..PDDSQLSDILKDARIPDSQDIGVNLTQNLSFDTVQKMIDGVFTPIFSQGTEDSLEKDILKTPGISTIYNGILGNGEETKKRTPKISDAFEPDLNTSGDVFDSDKSE
Human p63  MNFETSRCATLQYCPDPYIQRFVETPAHFSWKESYYRSTMS...........QSTQTNEF......LSPEVFQHIWD....FLEQ...............PICSVQPIDL
Human p73  MA..................................................QSTATSPD......GG.TTFEHLWS....SLEP..................DSTYFDL

Human p53
           30                40             50           60        70                80        90          100
Human p53  NNVLSPL.......PSQAMDDLMLS.....PDDIEQWFT...EDPGPDEAPRMPEAAPPVAPAP........AAPTPAAPAPAPSWPLSS..SVPSQKTY.Q.G......
Mouse p53  EDILP.........SPHCMDDLLLP......QDVEEFFE...G...PSEALRVSGAPAAQDPVT........ETPGPVAPAPATPWPLSS..FVPSQKTY.Q.G......
Fly p53    ...IPKTVE.VSGSELT.............TEPMAFLQG..LN...SGNLMQFSQ...................QSVLREMMLQDIQIQAN.TLPKLENHNI.G......
Worm p53   DGLMND.ES..YLSNTTLSQVVLD......SQKYEYLRV...R...TEEEQQLVIEKRARERFI..................RKSMKIAE.ETALSYEND.GSRELSETM
Human p63  NFVDEPSEDGATNKIEISMDCIRMQDSDLSDPMWPQYTNLGLLNSM...DQQIQNGSSSTSPYNTDHAQNSVTAPSPYAQPSSTFDALSPSPAIPSNTDY.P.G......
Human p73  PQSSRGNNE.VVGGTDSSMDVFHLEG..MTTSVMAQFN...LLSST...MDQMSSRAASASPYTPEHAA.SVPTHSPYAQPSSTFDTMSPAPVIPSNTDY.P.G......

                                                 S1           S2      S2'       S3                 S4
Human p53
                                              110       120         130       140       150           160
Human p53  .......................................SYGFRLGFLHSGTAKSVTCTYSPA...LNKMFCQLAKTCPVQLWVDST...PP.PGTRVRAMAIYKQSQH.
Mouse p53  .......................................NYGFHLGFLQSGTAKSVMCTYSPP...LNKLFCQLAKTCPVQLWVSAT...PP.AGSRVRAMAIYKKSQH.
Fly p53    .......................................GYCFSMVLDE..PPKS.LWMYSIP...LNKLYIRMNKAFNVDVQFKSK...MPIQPLNLRVFLCF..SND.
Worm p53   TQKVTQMDFTETNVPFDGNDESSNLAVRVQSDMNLNEDCEKWMEIDVLKQKVAKSSDMAFAISSEHEKYLWTKMGCLVPIQVKWKLDKRHFN.SNLSLRIRFVKYDKKEN
Human p63  .......................................PHSFDVSFQQSSTAKSATWTYSTE...LKKLYCQIAKTCPIQIKVMTP...PP.QGAVIRAMPVYKKAEH.
Human p73  .......................................PHHFEVTFQQSSTAKSATWTYSPL...LKKLYCQIAKTCPIQIKVSTP...PP.PGTAIRAMPVYKKAEH.

              η1        H1                  S5        S6               S7                   S8                 S9
Human p53  .......
                  170       180         190       200             210       220           230       240       250
Human p53  .......MTEVVRRCPHHERCSDSD..GLAPPQHLIRVEGNL.RVEYLD....DRNTFRHSVVVPYEPPE....VGSDCTTIHYNYMCNSSCMGGMNR.RPILTIITLED
Mouse p53  .......MTEVVRRCPHHERCSDGD..GLAPPQHLIRVEGNL.YPEYLE....DRQTFRHSVVVPYEPPE....AGSEYTTIHYKYMCNSSCMGGMNR.RPILTIITLED
Fly p53    .......VSAPVVRCQNHLSVEPLTANNAKMRESLLRSENPN..SVYCGNAQGKGISERFSVVVPLNMSRSVTRSGLTRQTLAFKFVCQNSCIGRK....ETSLVFCLEK
Worm p53   VEYAIRNPRSDVMKCRSHTEREQH.....FPFDSFFYIRNSEHEFSYSA....E...KGSTFTLIMY.......PGAVQANFDIIFMCQEKCLDLDDRRKTMCLAVFLDD
Human p63  .......VTEVVKRCPNHELSREFNEGQIAPPSHLIRVEGNS.HAQYVE....DPITGRQSVLVPYEPPQ....VGTEFTTVLYNFMCNSSCVGGMNR.RPILIIVTLET
Human p73  .......VTDVVKRCPNHELGRDFNEGQSAPASHLIRVEGNN.LSQYVD....DPVTGRQSVVVPYEPPQ....VGTEFTTILYNFMCNSSCVGGMNR.RPILIIITLEM

                 S10        H2
Human p53     -.
         260        270       280         290            300           310                                        320
Human p53  SSGNL.LGRNSFEVRVCACPGRDRRTEEEN..LRKKG...EP..HHELPP....GSTKRALPNNTS...............................SSP..QPKKKPLD
Mouse p53  SSGNL.LGRDSFEVRVCACPGRDRRTEEEN..FRKKE...VL..CPELPP....GSAKRALPTCTS...............................ASP..PQKKKPLD
Fly p53    ACGDI.VGQHVIHVKICTCPKRDRIQDERQ..LNSKKRKSVPEAAEEDEP....SKVRRCIAIKTED...............................TE..SNDSRDCD
Worm p53   ENGNEILHAYIKQVRIVAYPRRDWKNFCEREDAKQKD...FR..FPELPAYKKAS..LESINIKQEVNLENMFNVTNTTAQMEPSTSYSSPSNSNNRKRF..LNECDSPN
Human p63  RDGQV.LGRRCFEARICACPGRDRKADEDS..IRKQQ...VS..DSTKNG....DGTKRPFRQNTHGIQ............................MTS..IKKRRSPD
Human p73  RDGQV.LGRRSFEGRICACPGRDRKADEDH..YREQQ...AL..NESSAK..NGAASKRAFKQSPPAVP............................ALGAGVKKRRHGD

                                                               Tetra
Human p53
               330                                        340       350
Human p53  GEYFTLQI............................RGRERFEMFRELNEALELKDAQ............................AGKE....................
Mouse p53  GEYFTLKI............................RGRKRFEMFRELNEALELKDAH............................ATEE....................
Fly p53    DSAAEWNV............................SRTP..DGDYRLAITCPNKEWLLQSI....EGMIK....E......AAAEVLRN....................
Worm p53   NDYT.MMHRTPPVTGYASRLHGCVPPIETEHENCQSPSMKRSRCTNYSFRTLTLSTAE...YTKVVEFLAR..........EAK..VPRYTWVPTQVVSHILPTEGLERF
Human p63  DELLYLPV............................RGRETYEMLLKIKESLELMQYLPQHT....IETYRQQQQQQHQHLLQKQTSIQS....................
Human p73  EDTYYLQV............................RGRENFEILMKLKESLELMELVPQPL....VDSYRQQQQ.....LLQRPSHLQP....................

Human p53
           360                 370                                   380         390
Human p53  .PG....GSR......AHSSHLKSKK......G...................QSTS..RHKKLMFKTE..GPDSD...................................
Mouse p53  .SG....DSR......AHSSYLKTKK......G...................QSTS..RHKKTMVKKV..GPDSD...................................
Fly p53    .PN..QENLR................................................RHANKLLSLKK..RAYELP.................................
Worm p53   LTA....IKA......GHDSVLFNANGIYTMGDMIREFEKHNDIFERIGIDSSKLS..KYYEAFLSFYRIQEAMKLPK................................
Human p63  .PSSYGNSSPPLNKMNS.MNKLPSVS......Q...................LIN..PQQRNALTPTT..IPDGMGANIPMMGTHMPMAGDMNGLSPTQALPPPLSMPST
Human p73  .PS.YGPVLSPMNKVHGGMNKLPSVN......Q...................LVGQPPPHSSAATPNL..GPVGPGM.LNNHGHAVPANGEMS......SSHSAQSMVSG

Human p53

Human p53  ..............................................................................................................
Mouse p53  ..............................................................................................................
Fly p53    ..............................................................................................................
Worm p53   ..............................................................................................................
Human p63  SHCTPPPPYPTDCSIVSFLARLGCSSCLDYFTTQGLTTIYQIEHYSMDDLASLKIPEQFRHAIWKGILDHRQLHEFSSPSHLLRTPSSASTVSVG.SSETRGERVIDAVR
Human p73  SHCTPPPPYHADPSLVSFLTGLGCPNCIEYFTSQGLQSIYHLQNLTIEDLGALKIPEQYRMTIWRGLQDLKQGHDYSTAQQLLRS.SNAATISIGGSGELQRQRVMEAVH

Human p53

Human p53  .................................................
Mouse p53  .................................................
Fly p53    .................................................
Worm p53   .................................................
Human p63  FTLRQTISFPPR.......DEWNDFNFDMDARRNKQQRIKEEGE.....
Human p73  FRVRHTITIPNRGGPGGGPDEWADFGFDLPDCKARKQPIKEEFTEAEIH
```

Figure S4. Structure-Guided Sequence Alignment of p53 Orthologs and Paralogs, Related to Figure 4. The amino-acid sequences of human p53 (UniProt: P04637-1), mouse p53 (UniProt: P02340-1), fly p53 (UniProt: Q9N6D8-1), worm p53 (UniProt: Q20646-1), human p63 (UniProt: Q9H3D4-1), and human p73 (UniProt: O15350-1) were aligned using the Expresso module of the T-Coffee server. Identical residues among the homologs, zinc-binding residues, and ABP residues are highlighted in blue, black, and red, respectively. The human p53 residues frequently mutated in cancer are framed (structural in red whereas DNA-contact in green).

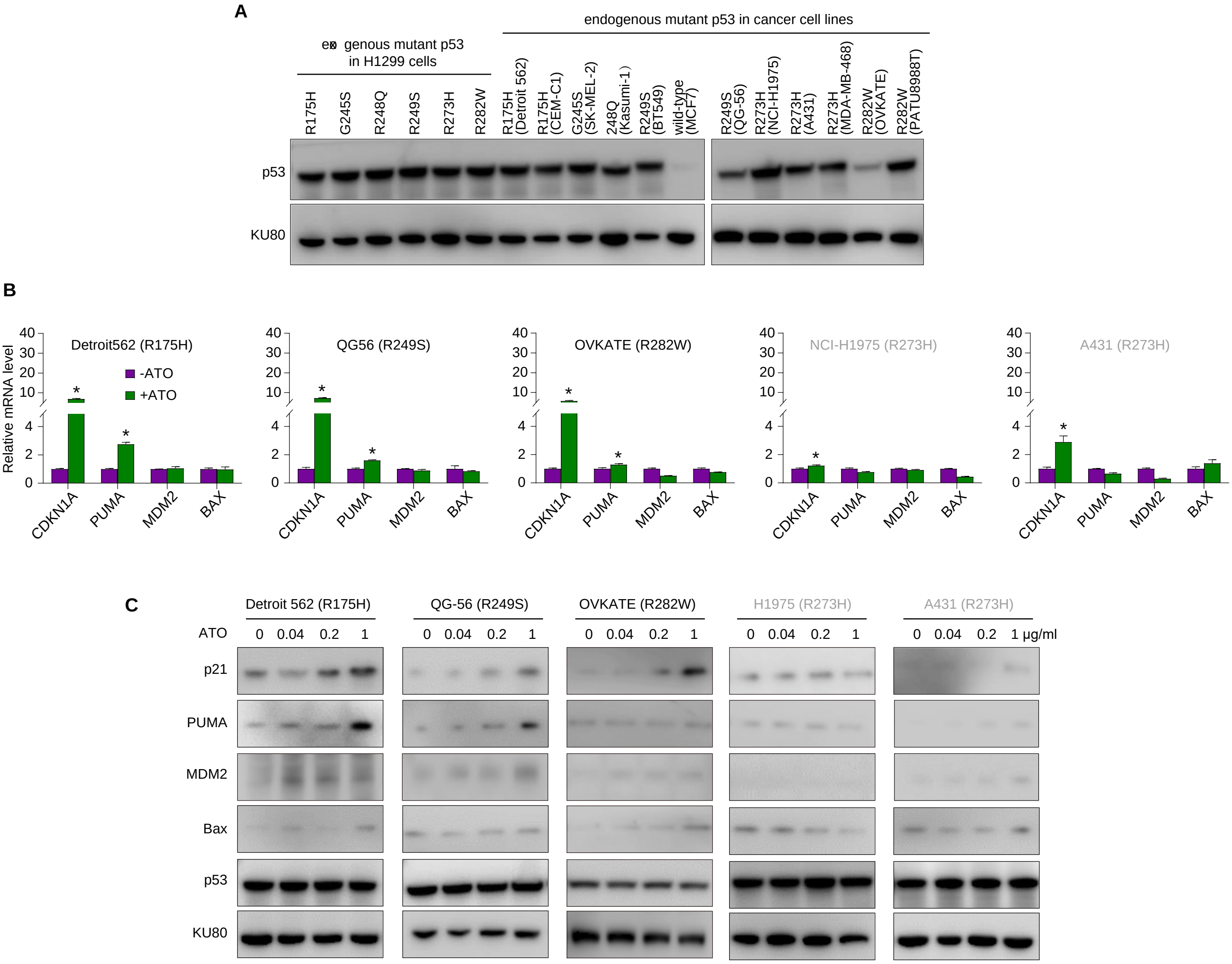

D

Fold change (FC) of p53 activities upon ATO treatment in 11 cancer cell lines with endogenous hotspot p53 mutants

	Cell lines	Cancer type	p53 mutation	1620/240 ratio (FC > 2?)	mRNA level (FC > 2?)				Protein level (FC > 2?)			
					CDKN1A	*PUMA*	*MDM2*	*Bax*	p21	PUMA	MDM2	Bax
1	CEM-C1	Acute lymphoblastic leukemia	R175H	Yes	Yes	Yes	Yes		Yes	Yes	Yes	
2	Detroit562	Pharyngeal carcinoma	R175H	Yes	Yes				Yes	Yes		Yes
3	SK-MEL-2	Malignant melanoma	G245S	Yes	Yes	Yes	Yes		Yes		Yes	
4	QG-56	Non-small cell lung cancer	R249S	Yes	Yes				Yes	Yes	Yes	
5	BT549	Mammary gland cancer	R249S	Yes	Yes	Yes			Yes			
6	OVKATE	Ovarian cancer	R282W	Yes	Yes				Yes			Yes
7	PATU8988T	Pancreatic adenocarcinoma	R282W	Yes	Yes				Yes	Yes	Yes	Yes
8	Kasumi	Acute myeloblastic leukemia	R248Q			Yes					Yes	
9	A431	Epidermis cancer	R273H		Yes				Yes	Yes		
10	MDA-MB-468	Mammary gland cancer	R273H									
11	NCI-H1975	Non-small cell lung cancer	R273H									

(legend on next page)

Figure S5. Transcriptional Reactivation by ATO, Related to Figure 5.
(**A**) Protein level of exogenous and endogenous p53 in the whole-cell lysate determined by immunoblotting.
(**B** and **C**) mRNA levels (B) and protein levels (C) determined as in Figure 5F and 5G, respectively. In (B), OVKATE cell line with relatively high IC50 were treated with 2 μg/mL ATO. The others were treated with 1 μg/mL ATO (note the immunoblotting image of A431 is the same as Figure 7H).
(**D**) Fold change (FC) of p53 activities upon ATO treatment in the panel of 11 cancer cell lines with endogenous hotspot p53 mutants summarized from Figure 1I, 5F-5G, and S5B-S5C. In (B), bars represent mean ± s.d. (n = 3, *$P < 0.05$).

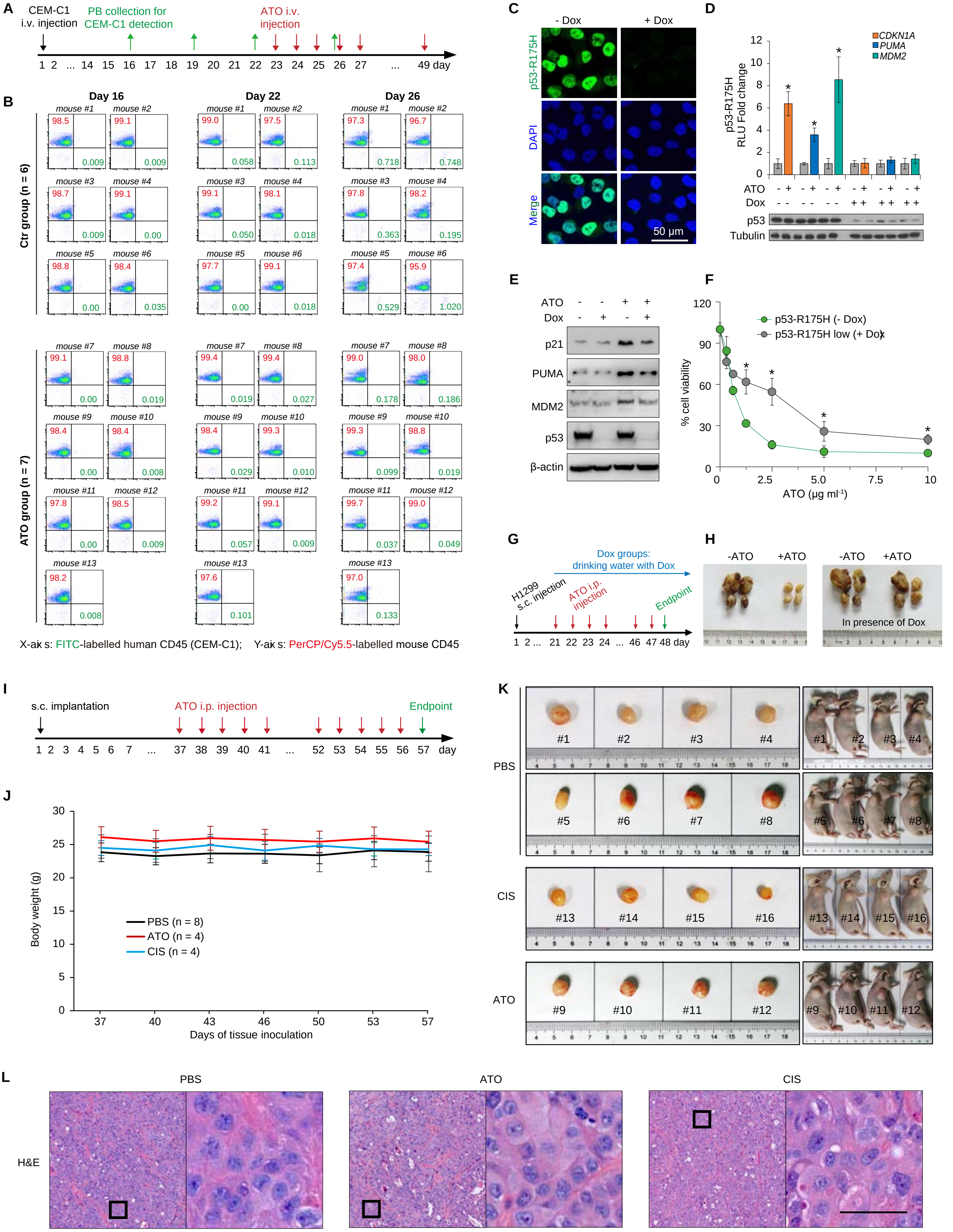

(legend on next page)

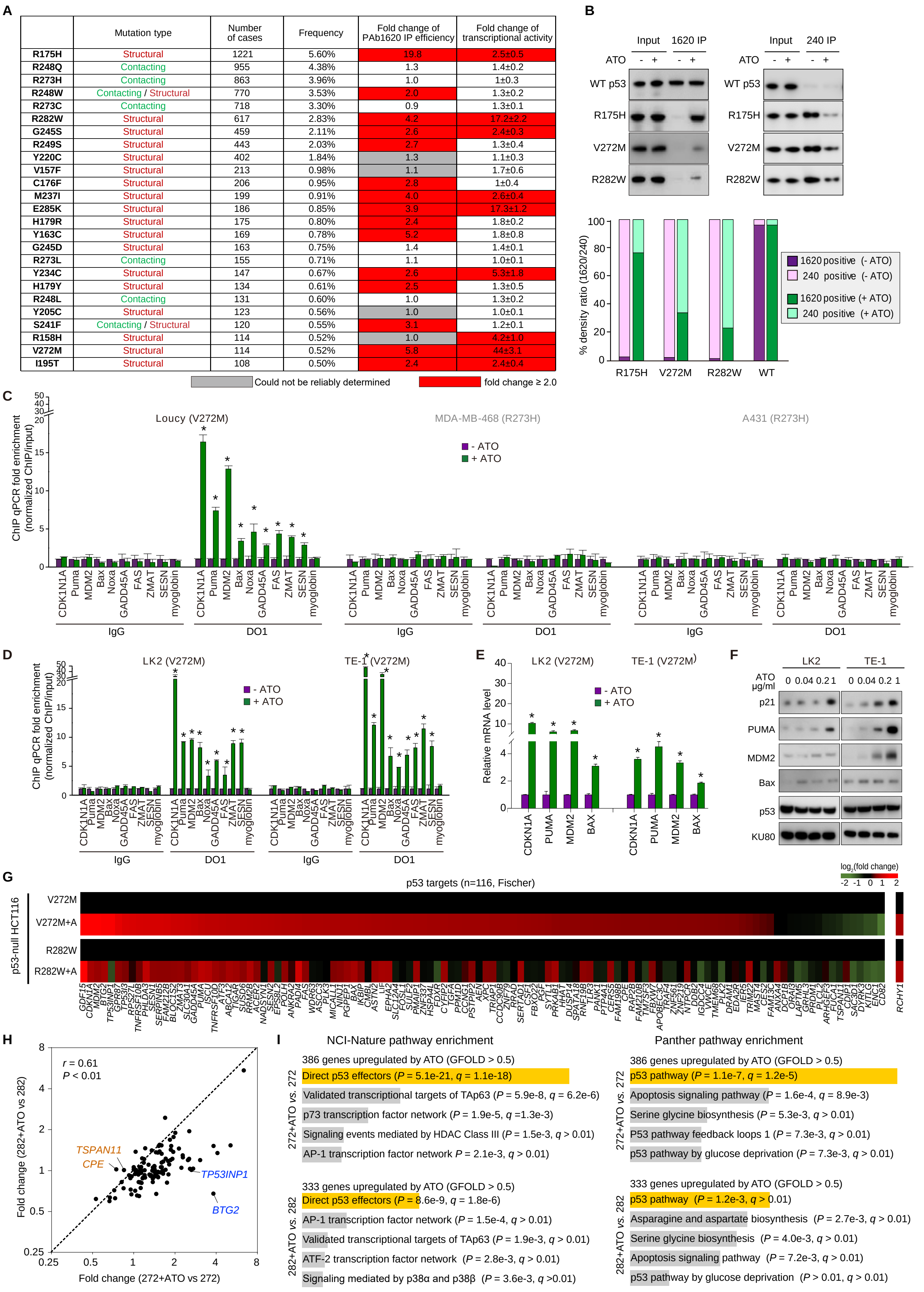

A

	Mutation type	Number of cases	Frequency	Fold change of PAb1620 IP efficiency	Fold change of transcriptional activity
R175H	Structural	1221	5.60%	19.8	2.5±0.5
R248Q	Contacting	955	4.38%	1.3	1.4±0.2
R273H	Contacting	863	3.96%	1.0	1±0.3
R248W	Contacting / Structural	770	3.53%	2.0	1.3±0.2
R273C	Contacting	718	3.30%	0.9	1.3±0.1
R282W	Structural	617	2.83%	4.2	17.2±2.2
G245S	Structural	459	2.11%	2.6	2.4±0.3
R249S	Structural	443	2.03%	2.7	1.3±0.4
Y220C	Structural	402	1.84%	1.3	1.1±0.3
V157F	Structural	213	0.98%	1.1	1.7±0.6
C176F	Structural	206	0.95%	2.8	1±0.4
M237I	Structural	199	0.91%	4.0	2.6±0.4
E285K	Structural	186	0.85%	3.9	17.3±1.2
H179R	Structural	175	0.80%	2.4	1.8±0.2
Y163C	Structural	169	0.78%	5.2	1.8±0.8
G245D	Structural	163	0.75%	1.4	1.4±0.1
R273L	Contacting	155	0.71%	1.1	1.0±0.1
Y234C	Structural	147	0.67%	2.6	5.3±1.8
H179Y	Structural	134	0.61%	2.5	1.3±0.5
R248L	Contacting	131	0.60%	1.0	1.3±0.2
Y205C	Structural	123	0.56%	1.0	1.0±0.1
S241F	Contacting / Structural	120	0.55%	3.1	1.2±0.1
R158H	Structural	114	0.52%	1.0	4.2±1.0
V272M	Structural	114	0.52%	5.8	44±3.1
I195T	Structural	108	0.50%	2.4	2.4±0.4

▨ Could not be reliably determined 🟥 fold change ≥ 2.0

I

NCI-Nature pathway enrichment

272+ATO vs. 272

386 genes upregulated by ATO (GFOLD > 0.5)

Direct p53 effectors (P = 5.1e-21, q = 1.1e-18)
Validated transcriptional targets of TAp63 (P = 5.9e-8, q = 6.2e-6)
p73 transcription factor network (P = 1.9e-5, q =1.3e-3)
Signaling events mediated by HDAC Class III (P = 1.5e-3, q > 0.01)
AP-1 transcription factor network P = 2.1e-3, q > 0.01)

282+ATO vs. 282

333 genes upregulated by ATO (GFOLD > 0.5)

Direct p53 effectors (P = 8.6e-9, q = 1.8e-6)
AP-1 transcription factor network (P = 1.5e-4, q > 0.01)
Validated transcriptional targets of TAp63 (P = 1.9e-3, q > 0.01)
ATF-2 transcription factor network (P = 2.8e-3, q > 0.01)
Signaling mediated by p38α and p38β (P = 3.6e-3, q >0.01)

Panther pathway enrichment

272+ATO vs. 272

386 genes upregulated by ATO (GFOLD > 0.5)

p53 pathway (P = 1.1e-7, q = 1.2e-5)
Apoptosis signaling pathway (P = 1.6e-4, q = 8.9e-3)
Serine glycine biosynthesis (P = 5.3e-3, q > 0.01)
P53 pathway feedback loops 1 (P = 7.3e-3, q > 0.01)
p53 pathway by glucose deprivation (P = 7.3e-3, q > 0.01)

282+ATO vs. 282

333 genes upregulated by ATO (GFOLD > 0.5)

p53 pathway (P = 1.2e-3, q > 0.01)
Asparagine and aspartate biosynthesis (P = 2.7e-3, q > 0.01)
Serine glycine biosynthesis (P = 4.0e-3, q > 0.01)
Apoptosis signaling pathway (P = 7.2e-3, q > 0.01)
p53 pathway by glucose deprivation (P > 0.01, q > 0.01)

(legend on next page)

Figure S7. Applicable Spectrum of p53 Mutations, Related to Figure 7.
(**A**) Summary of ATO rescue for the 25 most frequent p53 mutations. Data were derived from Figure 7B and 7C.
(**B**) PAb1620 and PAb240 IP assay for the indicated p53 mutants in H1299 cells.
(**C**) CHIP-qPCR determination as in Figure 7F, with more targets shown.
(**D**–**F**) Responses of p53 targets in ATO-treated LK2 and TE-1 cell lines as in Figure 7F–7H.
(**G**–**I**) RNA-seq result-based analysis as in Figure 7I. (G) Heat map as in Figure 7I, with each p53 targeted genes indicated. (**H**) dot plot shows the RPKM fold change upon ATO treatment. (I) The indicated pathway enrichments for ATO-upregulated genes (GFOLD > 1) against the human genome. In (C)–(E), bars represent mean ± s.d. (n = 3, *$P < 0.05$).